

SPITZER observations of Abell 1763. III. The infrared luminosity function in different supercluster environments

A. Biviano¹, D. Fadda², F. Durret^{3,4}, L.O.V. Edwards², F. Marleau⁵

¹ INAF/Osservatorio Astronomico di Trieste, via G. B. Tiepolo 11, I-34131, Trieste, Italy

² NASA Herschel Science Center, Caltech 100-22, Pasadena, CA 91125, USA

³ UPMC Université Paris 06, UMR 7095, Institut d'Astrophysique de Paris, 98bis Bd Arago, F-75014 Paris

⁴ CNRS, UMR 7095, Institut d'Astrophysique de Paris, 98bis Bd Arago, F-75014 Paris, France

⁵ Department of Astronomy and Astrophysics, University of Toronto, 50 Saint George Street, Toronto, ON M5S 3H4, Canada

Received / Accepted

ABSTRACT

Context. The study of galaxy luminosity functions (LFs) in different environments provides powerful constraints on the physics of galaxy evolution. The infrared (IR) LF is a particularly useful tool since it is directly related to the distribution of galaxy star-formation rates (SFRs).

Aims. We aim to determine the galaxy IR LF as a function of the environment in a supercluster at redshift 0.23 to shed light on the processes driving galaxy evolution in and around clusters.

Methods. We base our analysis on multi-wavelength data, which include optical, near-IR, and mid- to far-IR photometry, as well as redshifts from optical spectroscopy. We identify 467 supercluster members in a sample of 24- μ m-selected galaxies, on the basis of their spectroscopic (153) and photometric (314) redshifts. IR luminosities and stellar masses are determined for supercluster members via spectral energy distribution fitting. Galaxies with active galactic nuclei are identified by a variety of methods and excluded from the sample. SFRs are obtained for the 432 remaining galaxies from their IR luminosities via the Kennicutt relation.

Results. We determine the IR LF of the whole supercluster as well as the IR LFs of three different regions in the supercluster: the cluster core, a large-scale filament, and the cluster outskirts (excluding the filament). A comparison of the IR LFs of the three regions, normalized by the average number densities of r -band selected normal galaxies, shows that the filament (respectively, the core) contains the highest (respectively, the lowest) fraction of IR-emitting galaxies at all levels of IR luminosities, and the highest (respectively, the lowest) total SFR normalized by optical galaxy richness. Luminous IR galaxies (LIRGs) are almost absent in the core region. The relation between galaxy specific SFRs and stellar masses does not depend on the environment, and it indicates that most supercluster LIRGs are rather massive galaxies with relatively low specific SFRs. A comparison with previous IR LF determinations from the literature confirms that the mass-normalized total SFR in clusters increases with redshift, but more rapidly than previously suggested for redshifts $\lesssim 0.4$.

Conclusions. The IR LF shows an environmental dependence that is not simply related to the local galaxy density. The filament, an intermediate-density region in the A1763 supercluster, contains the highest fraction of IR-emitting galaxies. We interpret our findings within a possible scenario for the evolution of galaxies in and around clusters.

Key words. Galaxies: luminosity function - Galaxies: clusters: general - Galaxies: clusters: Abell 1763 - Galaxies: evolution - Galaxies: starburst

1. Introduction

The distribution of galaxy luminosities, i.e. the galaxy luminosity function (LF), and its environmental dependence have often been used to provide strong constraints on theories of galaxy evolution (see e.g. the investigations of Zucca et al. 2009; Merluzzi et al. 2010; Peng et al. 2010). Galaxy environment can be important in shaping several galaxy properties, such as colors, morphologies, and star-formation rates (SFRs; see e.g. Biviano 2008; Gavazzi 2009, for reviews). Since galaxy SFRs are strictly related to their total infrared (IR) emission (Kennicutt 1998), powerful constraints on how galaxies evolve in relation to their environment are expected to be obtained from the analysis of the galaxy IR LFs.

Following early studies of the IR properties of cluster galaxies with *IRAS* and *ISO* (see Metcalfe et al. 2005, and references therein), the *Spitzer Space Telescope* (Werner et al. 2004), the

AKARI satellite (Murakami et al. 2007), and now the *Herschel Space Observatory* (Pilbratt et al. 2010), have only recently allowed a precise derivation of galaxy IR LFs at various redshifts and in various environments in a precise way.

Most determinations of galaxy IR LFs in cluster and supercluster environments have so far been based on *Spitzer* data. Bai et al. (2006, 2009) analyzed the IR LFs of the rich nearby clusters Coma and A3266. According to their analysis, the bright end of the IR LF has a universal form for local rich clusters, and cluster and field IR LFs have similar values of their characteristic luminosities, L_{IR}^* . Nearby rich clusters have a lower star-forming galaxy fraction than field galaxies, although this fraction increases with cluster-centric distance.

These results were confirmed by Finn et al. (2010), who analyzed a larger sample of clusters in the redshift range $0.4 \leq z \leq 0.9$. They noted the similarity in the shape of the cluster and field IR LFs, and confirmed that there is an increase in the

Send offprint requests to: Andrea Biviano, biviano@oats.inaf.it

fraction of luminous IR galaxies (LIRGs¹) with cluster-centric distance, out to 1.5 virial radii², where it is still below the field value. Temporin et al. (2009) also noted the absence of LIRGs from the central regions of a sample of 32 X-ray selected clusters. Recent *Herschel* observations provide evidence of a lack of IR galaxies not only at the bright end but also the faint end of the IR LF of the nearby Virgo cluster relative to the field (Davies et al. 2010).

The environmental dependence of the fraction of high-SFR galaxies may not be a simple function of cluster-centric distance. Fadda et al. (2008, Paper 0) detected a large-scale filament³ in the IR, connecting a rich and a poor cluster at $z \sim 0.2$. They observed that the fraction of high-SFR galaxies is largest in the filament, i.e. larger than in the cluster core, but also larger than in other, lower density, regions of the supercluster. The filament detected by Fadda et al. (2008) was the first to be found via IR observations (with *Spitzer*); *Herschel* observations have recently revealed other large-scale structure filaments traced by IR-emitting galaxies (Haines et al. 2010; Pereira et al. 2010), but the analysis of their galaxy populations is still ongoing.

Koyama et al. (2008, 2010) observed that the medium- and low-density regions of another (more distant, $z \sim 0.8$) supercluster host comparable fractions of star-forming galaxies, while red mid-IR emitters are preferentially located in medium-density environments, such as galaxy filaments. Both Fadda et al. (2008) and Koyama et al. (2010) argued that star-formation is triggered in galaxies in the infall regions around clusters. Gallazzi et al. (2009) came to the same conclusion after analyzing the IR galaxy population in a $z = 0.165$ supercluster. They also found that while the IR galaxies prefer to live in medium-density environments, their SFRs are not particularly high for their stellar masses (M_*), i.e. they have normal specific SFRs ($sSFR \equiv SFR/M_*$).

Groups are another environment characterized, as in the case of filaments, by galaxy densities intermediate between cluster cores and the field. Tran et al. (2009) determined the IR LFs of a rich galaxy cluster and four galaxy groups at $z \sim 0.35$. The fraction of galaxies with a high SFR was found to be four times larger in the groups than in the cluster, or equivalently, the group IR LF has an excess at the bright end relative to the cluster IR LF. On the basis of this result, Chung et al. (2010) interpreted the excess of bright IR sources in the IR LF of the Bullet cluster ($z \sim 0.3$) as being due to the galaxy population in an infalling group (the “bullet” itself).

The IR LF not only depends on the environment, but also on redshift. Bai et al. (2009) compared the average IR LFs of two nearby ($z \leq 0.06$) and two distant ($z \sim 0.8$) clusters (using the data of Bai et al. 2006, 2007). They concluded that there is an evolution with z of both the characteristic luminosity L_{IR}^* and the normalization of the LF, n^* , such that higher- z clusters contain more and brighter IR galaxies. This evolution of the cluster IR LF results in a rapid increase with

z in the total SFR of cluster galaxies divided by the total cluster mass, $\Sigma SFR/mass \propto (1+z)^{5.3}$, a result anticipated by Geach et al. (2006), who suggested an even faster evolution. Another way to characterize this evolution is to look at the fraction of IR-emitting galaxies (above a given IR luminosity, L_{IR}) as a function of z . This fraction is observed to increase with z , a phenomenon called “the IR Butcher-Oemler effect” (Saintonge et al. 2008; Haines et al. 2009a; Temporin et al. 2009), since it is reminiscent of the increasing fraction of blue cluster galaxies with z (Butcher & Oemler 1984). The increasing fraction of LIRGs with z appears however to be a common phenomenon in cluster and field environments (Finn et al. 2010).

To shed light on the physical processes responsible for the environmental and redshift dependence of the IR LF, we present a study of the IR LF of galaxies in the $z = 0.23$ A1763–A1770 supercluster. Our analysis is restricted to the part of the supercluster that includes the rich cluster A1763, part of the filament connecting the two clusters (see Paper 0), and the outskirts region around the A1763 cluster core, excluding the filament itself (see Sect. 3.3).

In Sect. 2, we describe our observational data-set (Sect. 2.1), assign supercluster memberships to the observed IR galaxies (Sect. 2.2), and determine their total IR luminosities (Sect. 2.3) and stellar masses (Sect. 2.4). In Sect. 3, we describe the corrections applied to the IR galaxy counts (Sect. 3.1) to determine the supercluster IR LF (Sect. 3.2). We then determine the corrected IR LFs of three different regions of the A1763 supercluster to explore environmental effects (Sect. 3.3). We compare our results with previous results from the literature in Sect. 3.4. In Sect. 4, we discuss our results and summarize them in Sect. 5.

We adopt $H_0 = 70 \text{ km s}^{-1} \text{ Mpc}^{-1}$, $\Omega_m = 0.3$, $\Omega_\Lambda = 0.7$ throughout this paper. In this cosmology, 1 arcmin corresponds to 222 kpc at the cluster redshift.

2. The data set

2.1. Observations

The data used in this study were obtained as part of a multi-wavelength observational campaign conducted with several space- and ground-based telescopes. Details are provided in Edwards et al. (2010a, Paper 1). Here we summarize the main characteristics of the data set. A field of $\sim 40 \times 55 \text{ arcmin}^2$ centered on the A1763 cluster was covered by MIPS 24, 70, and $160 \mu\text{m}$ observations from *Spitzer*. Two similar fields were also covered by IRAC 3.6, 4.5, 5.8, and $8.0 \mu\text{m}$ observations from *Spitzer*. A similar area was observed with the Palomar 200 inch telescope in the r' , J , H , and K_s filters. In addition, we obtained spectroscopic observations for galaxies across the supercluster region, using the KPNO WIYN and TNG telescopes (paper in preparation). Finally, the A1763 field was covered by the *Sloan Digital Sky Survey* (SDSS hereafter) in the u' , g' , r' , i' , z' photometric bands, and we collected all data available in the A1763 field from the SDSS Seventh Data Release (DR7 hereafter). We use Petrosian magnitudes and total fluxes in the following analyses.

Our sample contains 10876 objects identified at $24 \mu\text{m}$ in the MIPS field. The observational technique as well as the depth of our MIPS observations are very similar to those of the “verification survey” in the *Spitzer Space Telescope* Extragalactic First Look Survey (EFLS hereafter; Fadda et al. 2006). For this reason, we assume that the completeness and purity functions of the EFLS and those of our survey are identical. This is a conservative assumption because the EFLS sources were selected using

¹ LIRGs are galaxies with a total (8–1000 μm) IR luminosity $L_{IR} \geq 10^{11} L_\odot$.

² The cluster virial radius, r_{200} , is the radius within which the enclosed average mass density of a cluster is 200 times the critical density. The circular velocity v_{200} is defined as $v_{200} = 10 H(z) r_{200}$. The virial mass M_{200} follows from the two previous quantities, $M_{200} = r_{200} v_{200}^2 / G$.

³ In Paper 0, we originally identified two filaments, running almost parallel in projection in the sky, but slightly separated along line-of-sight velocity space. Subsequent spectroscopic observations indicate that the two filaments merge into one at large distances from the A1763 cluster core. For simplicity, we therefore here refer to a single filament in the supercluster.

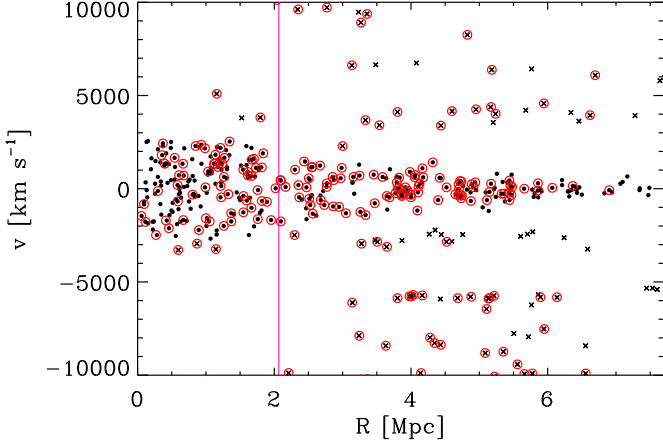


Fig. 1. The rest-frame velocities versus cluster-centric distances of the galaxies with available z . The vertical solid pink line marks the distance to the cluster virial radius, r_{200} . Black dots represent the 357 galaxies selected as supercluster members by the algorithm of Mamon et al. (2010), interlopers are marked by X's. Red circles identify $24\ \mu\text{m}$ emitters. 153 of them are selected as supercluster members.

the peak signal-to-noise ratio, while here sources were selected using the aperture signal-to-noise ratio, which is more efficient in the rejection of false detections. Completeness, C_{det} , is defined as the fraction of real sources that are detected, and purity, P_{det} , is defined as the fraction of real sources among the detected ones. The completeness is $C_{\text{det}} \sim 80\%$ at $24\ \mu\text{m}$ flux densities $f_{24} = 0.2\ \text{mJy}$, and close to 100% at $f_{24} > 0.4\ \text{mJy}$. The purity is $P_{\text{det}} \sim 95\%$ at $f_{24} \geq 0.2\ \text{mJy}$ and above (see Fig. 13 in Fadda et al. 2006).

We base the determination of the IR LFs on the sample of $24\ \mu\text{m}$ -detected IR-emitting galaxies, since our $70\ \mu\text{m}$ and $160\ \mu\text{m}$ observations are not as deep. About 60% of the $24\ \mu\text{m}$ -selected objects have $f_{24} \geq 0.2\ \text{mJy}$ and therefore belong to the sample with $\geq 80\%$ completeness and $\sim 95\%$ purity. We use these completeness and purity estimates in the construction of the supercluster IR LF (see Sect. 3.1).

2.2. Supercluster membership

To define the supercluster membership of the galaxies in the cluster field, we use both spectroscopic (z) and photometric redshifts (z_p).

We use the algorithm of Mamon et al. (2010) to identify the supercluster members among the galaxies with available z . This algorithm tries to infer the galaxy cluster membership from the location of the galaxy in the cluster-centric distance – velocity diagram shown in Fig. 1, based on the modeling of the mass and anisotropy profiles of cluster-sized halos extracted from a cosmological numerical simulation. The procedure is more effective than traditional approaches (e.g. Yahil & Vidal 1977) in rejecting interlopers, while still preserving cluster members.

The galaxy rest-frame velocities with respect to the cluster mean velocity are obtained from the usual relation $v = c(z - \bar{z})/(1 + \bar{z})$ (Harrison & Noonan 1979), where $\bar{z} = 0.2314$ is obtained using the biweight estimator (Beers et al. 1990). We then obtain the galaxy projected distances from

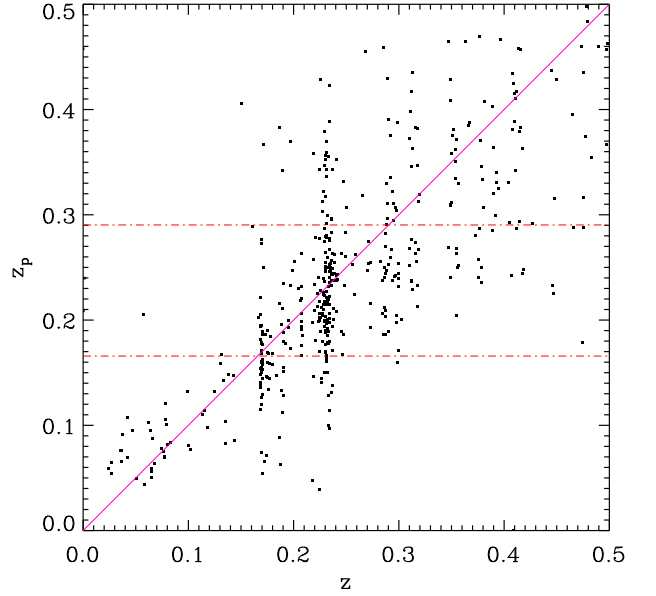


Fig. 2. SDSS DR7 photometric redshift z_p (Artificial Neural Network estimates, Oyaizu et al. 2008) versus spectroscopic redshift z for the IR-emitting galaxies with available z and z_p in the supercluster field (471 galaxies in the displayed z and z_p ranges). The solid pink line is the identity relation $z = z_p$. The dash-dotted red lines indicate the chosen z_p range for membership selection (see text and Fig. 3).

the cluster center, defined by its X-ray peak emission, $\text{RA}=13^{\text{h}}35^{\text{m}}17.96^{\text{s}}$, $\delta=40^{\circ}59'55.8''$ (Cavagnolo et al. 2009).

The algorithm of Mamon et al. (2010) requires initial estimates of the virial radius, r_{200} , and circular velocity, v_{200} , which we obtain from the cluster velocity dispersion estimate of Paper 0, by following Mauduit & Mamon (2007, Appendix A), and using the relation of Gao et al. (2008) to infer the concentration of the cluster mass-density distribution.

We run the procedure on the whole sample of 1364 objects with available redshift estimates in the supercluster field. The procedure is run iteratively until convergence on the number of selected members. We identify 357 supercluster members (they are shown as filled dots in Fig. 1). Other algorithms (e.g. den Hartog & Katgert 1996; Fadda et al. 1996) lead to very similar membership definitions. The average cluster redshift and velocity dispersion determined for this sample of supercluster members are $\bar{z} = 0.2315 \pm 0.0003$ and $\sigma_v = 1051^{+51}_{-54}\ \text{km s}^{-1}$. We use these values to estimate the cluster virial radius and circular velocity as before, finding $r_{200} = 2.066\ \text{Mpc}$ and $v_{200} = 1623\ \text{km s}^{-1}$, which do not differ significantly from the initially adopted values.

Of the 357 identified supercluster members, 153 are $24\ \mu\text{m}$ -emitters.

To estimate the supercluster membership for the subset of galaxies without z , we rely on z_p -estimates. We consider six different z_p -estimates for the galaxies in our sample. In particular, we consider the ANNz (Collister & Lahav 2004) and EAZY (Brammer et al. 2008) algorithms, as well as a χ^2 minimization fitting of the spectral energy distribution (SED, hereafter) of the galaxies in our sample using SED model templates from

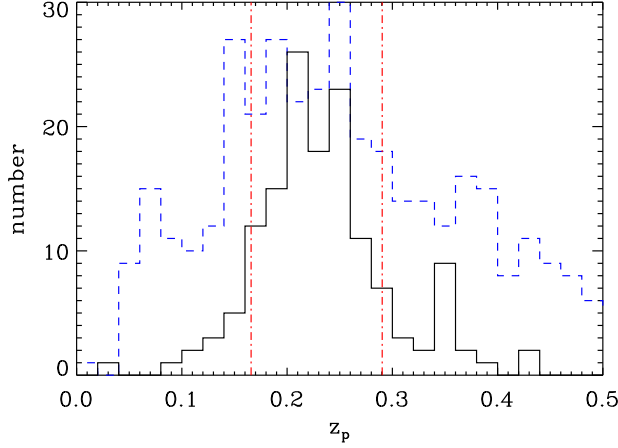


Fig. 3. The z_p distributions for the IR-emitting galaxies with available z in the supercluster field. The solid black (respectively, dashed blue) histogram represents the z_p distribution for the galaxies selected as members (respectively, not selected as members) on the basis of their z . The two vertical red dash-dotted lines identify the lower and upper z_p limits used to identify supercluster members in the sample of galaxies without z (not shown here).

Polletta et al. (2007). We also consider the three z_p estimates directly available from the SDSS DR7. Of these six z_p estimators, we finally adopt one of those provided in the SDSS DR7, that based on the Artificial Neural Network technique (Oyaizu et al. 2008). This estimator provides the tightest correlation between z and z_p for the subsample of galaxies in the A1763 field that have both quantities available (see Fig. 2).

To select the supercluster members in the sample of $24\ \mu\text{m}$ -emitters on the basis of their z_p , we define a z_p -range around the mean supercluster redshift. The lower and upper z_p -limits that define this selection range must be chosen in such a way as to maximize the number of real supercluster members with z_p within these limits, and, at the same time, minimize the number of background and foreground galaxies that also happen to have their z_p within these limits. The choice of these z_p -limits can only be based on the sample of galaxies with z_p and z , so that we can perform the most robust z_p -based membership selection possible based on the well-established spectroscopic membership.

We proceed as follows. We assume that the 153 supercluster members selected on the basis of their z are all real members. We then determine the z_p -distribution of these 153 galaxies (shown as a solid black histogram in Fig. 3), as well as the z_p -distribution of the galaxies with z in either the foreground or the background of the supercluster (dashed blue histogram in Fig. 3). Using the whole sample of galaxies with z and z_p , we define the purity and completeness to be, respectively⁴: $P_{\text{pm}} \equiv N_{\text{pm} \cap \text{zm}} / N_{\text{pm} \cap \text{z}}$ and $C_{\text{pm}} \equiv N_{\text{pm} \cap \text{zm}} / N_{\text{zm} \cap \text{p}}$, where $N_{\text{zm} \cap \text{p}}$ is the number of spectroscopically confirmed cluster members with available z_p , and $N_{\text{pm} \cap \text{z}}$ (respectively, $N_{\text{pm} \cap \text{zm}}$) is the number of galaxies with z (respectively, the number of spectroscopically confirmed cluster members) that have z_p within a given z_p -range. Following Knobel et al. (2009) we determine the optimal z_p range by mini-

⁴ For the sake of simplicity hereafter, we use the letter “p” in lieu of “ z_p ” in the subscripts.

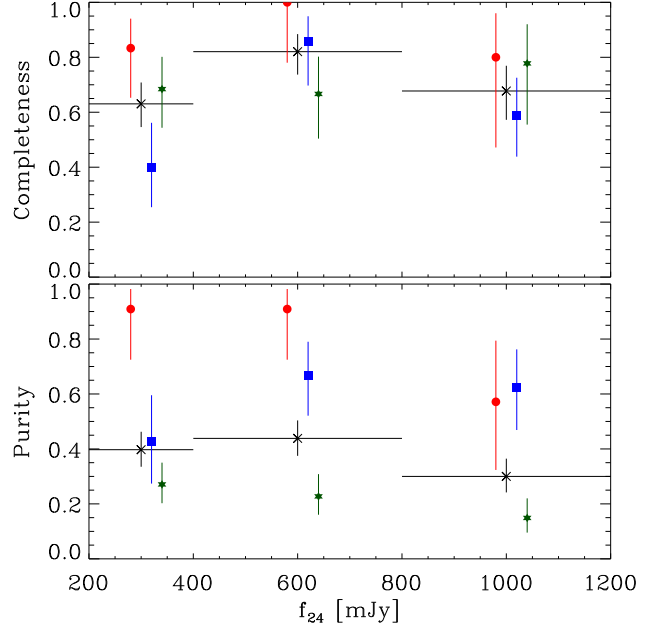


Fig. 4. Completeness (C_{pm}) and purity (P_{pm}) of the sample of IR-emitting supercluster members selected on the basis of their z_p ($0.166 \leq z_p \leq 0.290$), as a function of f_{24} . C_{pm} and P_{pm} are estimated using the sample of $24\ \mu\text{m}$ -emitters with both z and z_p available, and assuming the members selected on the basis of their z are all real members. The black X's are for the total sample. The red dots, blue squares, green stars are for the core, filament, and outskirts subsamples, respectively (see 3.3 for the definition of these subsamples). Horizontal bars indicate the f_{24} bin intervals. Vertical bars indicate $1\text{-}\sigma$ uncertainties.

mizing $\sqrt{(1 - P_{\text{pm}})^2 + (1 - C_{\text{pm}})^2}$. The minimum is obtained for $C_{\text{pm}} = 0.73$ and $P_{\text{pm}} = 0.42$, corresponding to the z_p -range $0.166\text{--}0.290$. The dependence of C_{pm} and P_{pm} on f_{24} is not very strong (see Fig. 4). Among the galaxies without z , 314 have z_p within this range.

In Fig. 2, the two red dashed lines indicate the chosen z_p -range. It can be seen that most of the supercluster galaxies fall in that range, but also many of the galaxies that belong to two other z -peaks, one at $z \sim 0.17$, another at $z \sim 0.29$. We consider whether it is possible to increase the purity of the sample of z_p -selected cluster members by identifying and then removing the galaxy structures responsible for these two z -peaks. The lower- z peak does not correspond to a concentrated structure in space. The higher- z peak does seem to correspond, at least partly, to a spatial concentration of galaxies, located at edge of the observed Spitzer field. However, removing the (small) region corresponding to this (presumed) galaxy concentration from our analysis has hardly any noticeable effect on the results presented in this paper.

In total, we select 467 IR-emitting galaxies as supercluster members, 153 on the basis of z , 314 on the basis of z_p . We base the derivation of the supercluster IR LF on both the total sample of members (the $z \cup z_p$ sample, hereafter), and the sample of z -selected members (the z sample, hereafter; see Sect. 3.2). Using both samples allows us to check the influence of possible systematic errors because the $z \cup z_p$ sample is affected by sig-

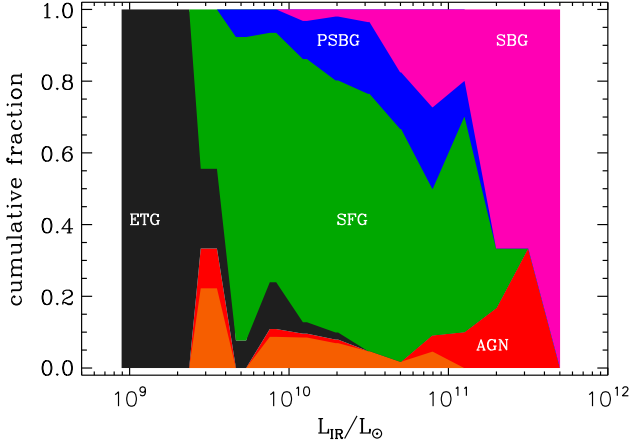


Fig. 5. The cumulative fractions of galaxies of different SED classes as a function of L_{IR} , for the $z \cup z_p$ sample. The pink, blue, green, and black-shaded regions correspond to the fractions of SBGs, PSBGs, SFGs, and ETGs, respectively (as labeled). The orange and red-shaded regions correspond to the fractions of SED-identified AGNs (mostly at low L_{IR}) and AGNs identified in Paper 2 from X-ray or radio emission, respectively.

nificant contamination by non-real members (low purity), while the z sample is affected by larger incompleteness than the $z \cup z_p$ sample.

2.3. Total infrared luminosities

To determine the total IR luminosities (L_{IR}) of the 467 supercluster members, we fit the galaxy SEDs with two sets of model templates, one from GRASIL (Silva et al. 1998), the other from Polletta et al. (2007). These templates span a wide range of galaxy types, with different formation redshifts, and were used in Paper 0 as well as (in part) in Biviano et al. (2004) and Coia et al. (2005a,b). In total, we consider 61 SED templates of galaxies of different ages and types, belonging to the following five classes:

- ETGs, early-type galaxies;
- SFGs, normal star-forming galaxies;
- SBGs, starburst galaxies;
- PSBGs, post-starburst galaxies;
- AGNs, active galactic nuclei.

We find the best-fit templates by comparing the template and observed fluxes via a χ^2 minimization procedure. To compute the template fluxes in the observed photometric bands, the templates are redshifted to the galaxy (photometric or spectroscopic) redshifts and convolved with the filter response curves. The minimization procedure is run interactively, allowing, when needed, the eye-rejection of deviant photometric data in the fits of individual galaxy SEDs. We finally determine L_{IR} by integrating the best-fit model SEDs over the 8–1000 μm rest-frame wavelength range.

Given the galaxy IR luminosities, we determine the galaxy SFRs using the relation of Kennicutt (1998), $\text{SFR}[\text{M}_{\odot}/\text{yr}] = 1.7 \cdot 10^{-10} \cdot L_{\text{IR}}/L_{\odot}$. This relation is clearly valid only when a galaxy IR luminosity is not dominated by the emission from an AGN. Since most galaxies in our sample lack

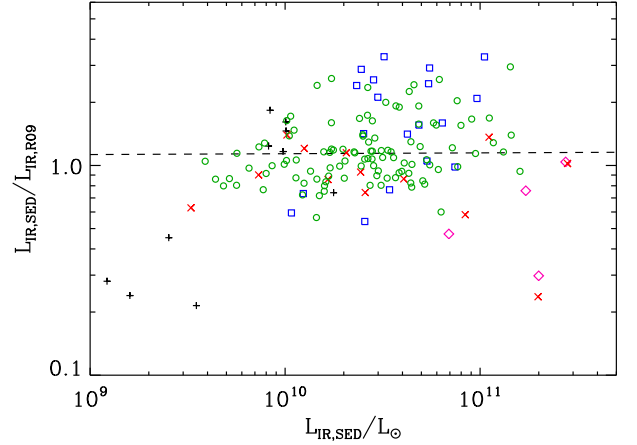


Fig. 6. Comparison of two IR luminosity estimates, $L_{\text{IR,SED}}/L_{\text{IR,R09}}$ versus $L_{\text{IR,SED}}$. Different symbols identify different galaxy SED classes. Black crosses for early-type galaxies (ETGs), red X's for active-galactic nuclei (AGNs), pink diamonds for starburst galaxies (SBGs), blue squares for post-starburst galaxies (PSBGs), and green circles for normal star-forming galaxies (SFGs). The dashed line is the biweight average ratio of the sample of non-AGN galaxies.

far-IR photometry, it may be difficult for us to distinguish AGNs from galaxies with IR emission dominated by star formation. It is therefore also worth considering other AGN diagnostics.

In Edwards et al. (2010b, Paper 2), we identified AGNs in the A1763 region using optical, radio, X-ray data, and IRAC colors. Nine of the AGNs identified in Paper 2 are in our sample, and only one of them has been classified as an AGN based on its SED. This is unsurprising, since AGNs become visible in different bands at different stages of their evolution (Hickox et al. 2009), and since the AGNs identified in Paper 2 in the IRAC color diagram are at the margin of the AGN-identification region (see Fig. 6 in Paper 2). We also adopt the AGN classification of Paper 2 for the 8 galaxies with non-AGN SED classification, bringing the total of AGNs in our sample to 35 (13 with available z). We are therefore confident we have identified most (if not all) galaxies with AGN-dominated IR emission.

The relative contribution of the different SED classes in different L_{IR} bins is shown in Fig. 5 for the $z \cup z_p$ sample (the equivalent figure for the z sample is very similar and not shown here). Fig. 5 shows that SBGs contribute mostly at high L_{IR} , but a significant fraction of the LIRGs are normal SFGs. The fraction of SFGs and of PSBGs increases at lower L_{IR} , and SFGs dominate at intermediate L_{IR} . Most of the galaxies at the faint-end of the IR LF are ETGs. In line with previous results and with our previous analysis (Paper 2), we find the contribution of AGNs to the IR LF of A1763 to be small (e.g. Geach et al. 2009; Krick et al. 2009; Chung et al. 2010), and to increase with L_{IR} (e.g. Bothwell et al. 2011; Goto et al. 2011).

In order to check the robustness of our SED-based L_{IR} estimates we consider alternative estimates based on direct relations between f_{24} and L_{IR} , from Rieke et al. (2009) and Lee et al. (2010). When comparing the different L_{IR} estimates, we only consider the subsample of 140 spectroscopically confirmed non-AGN A1763 members, to be sure that the comparisons are unaffected by the additional scatter introduced by photometric red-

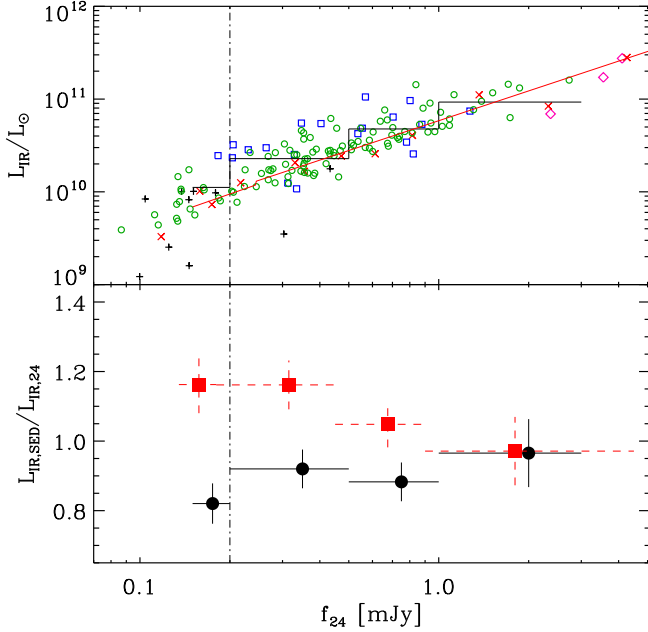


Fig. 7. *Upper panel:* $L_{\text{IR,SED}}$ versus f_{24} for the galaxies of the z sample (spectroscopically confirmed supercluster members). The dash-dotted line indicates the completeness limit of 0.2 mJy (see Sect. 2). The solid red line indicates the relation of Rieke et al. (2009), and the solid black histogram the tabulated values of $L_{\text{IR,SED}}$ for different f_{24} from Lee et al. (2010), scaled from their lowest redshift bin to the average redshift of A1763. The meaning of the symbols is the same as in Fig. 6. *Lower panel:* ratios of the biweight averages of $L_{\text{IR,SED}}$ (AGNs excluded) to either the tabulated values $L_{\text{IR,L10}}$ (black dots), or the biweight averages of $L_{\text{IR,R09}}$ (red squares), in bins of f_{24} . In the y-axis label, we generically use the notation $L_{\text{IR,24}}$ to refer to either $L_{\text{IR,R09}}$ or $L_{\text{IR,L10}}$. Vertical bars are 1σ uncertainties in the means; horizontal bars indicate the bin ranges. The red squares have been slightly displaced along the horizontal axis for clarity.

shift errors. In discussing the results of these comparisons, we refer to our L_{IR} estimates as $L_{\text{IR,SED}}$, to the f_{24} -based L_{IR} estimates of Rieke et al. (2009) as $L_{\text{IR,R09}}$, and to the f_{24} -based L_{IR} estimates of Lee et al. (2010) as $L_{\text{IR,L10}}$.

The relation between $L_{\text{IR,R09}}$ and f_{24} is obtained by combining eqs. (10), (11), (14), and (A6) in Rieke et al. (2009), and by interpolating the values of Table 1 in that same paper at the mean redshift of A1763. Fig. 6 shows $L_{\text{IR,SED}}/L_{\text{IR,R09}}$ versus (vs.) $L_{\text{IR,SED}}$ for our sample. There is a reasonably good agreement between the two L_{IR} estimates, with a rather small systematic offset, $\langle L_{\text{IR,SED}}/L_{\text{IR,R09}} \rangle = 1.12 \pm 0.05$ (biweight average, see Beers et al. 1990).

Lee et al. (2010) adopted an empirical approach to the L_{IR} estimate from 24 μm flux densities. They stacked 70 and 160 μm images (taken with *Spitzer*) around sources detected at 24 μm , in different redshift and f_{24} bins. They then determined L_{IR} by fitting the SEDs of the median flux densities in the stacks. To compare our L_{IR} estimates to theirs, we scale their lowest- z bin values (at an average redshift $z = 0.263$, private communication by N. Lee) to the redshift of A1763, and we estimate the average L_{IR} of our spectroscopically confirmed, non-AGN, A1763 members in the same f_{24} bins used by Lee et al. (2010).

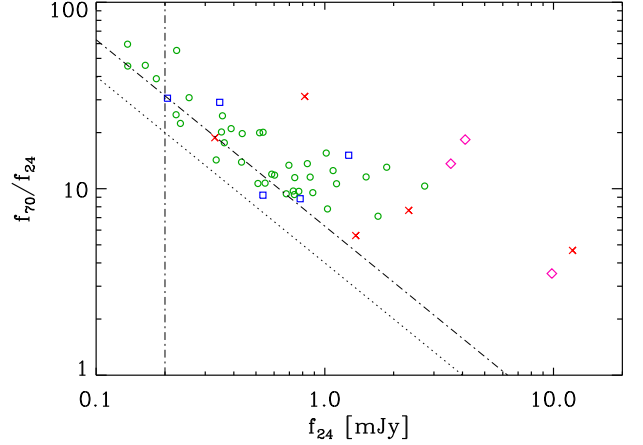


Fig. 8. The ratio between the 70 and 24 μm flux densities, f_{70}/f_{24} as a function of f_{24} for the sample of spectroscopically confirmed supercluster members with available f_{70} . The vertical line indicates the completeness limit of 0.2 mJy. The two parallel dotted and dash-dotted lines indicate the detection and, respectively, completeness limit of the 70 μm catalog, 4.0 and 6.3 mJy, respectively. See Fig. 6 for the meaning of the symbols.

In the upper panel of Fig. 7, we show the $L_{\text{IR,SED}}$ vs. f_{24} value for the galaxies of our z sample (spectroscopically confirmed supercluster members), as well as the relations of Rieke et al. (2009) and Lee et al. (2010). In the lower panel of the same figure, we display the ratios of the biweight averages of $L_{\text{IR,SED}}$ to either the tabulated values $L_{\text{IR,L10}}$ or the biweight averages of $L_{\text{IR,R09}}$ in bins of f_{24} . It appears that our L_{IR} -estimates are in-between those obtained using the relations of Rieke et al. (2009) and Lee et al. (2010). Overall, these comparisons lend support to the accuracy of our L_{IR} -estimates.

The small systematic offsets we observe between our $L_{\text{IR,SED}}$ and either the estimates of Rieke et al. (2009) or those of Lee et al. (2010) may occur if the SEDs of some galaxies in high-density regions are not represented by the used model templates, and if they are atypical of the median SED of the field galaxy population sampled by Lee et al. (2010). We note in particular that PSBGs from our z sample tend to have $L_{\text{IR,SED}} > L_{\text{IR,R09}}$, and SBGs $L_{\text{IR,SED}} < L_{\text{IR,R09}}$ (see Fig. 6). Moreover, we observe that $L_{\text{IR,SED}}/L_{\text{IR,R09}}$ increases with increasing 70 to 24 μm flux density ratio, a correlation that is significant at the 99% confidence level. This correlation is similar to that observed by Rawle et al. (2010) for galaxies in the Bullet cluster, between the 100 to 24 μm flux density ratio and the ratio of the SFR obtained from SED fitting, to the SFR obtained from f_{24} via the relations of Rieke et al. (2009). Rawle et al. (2010) pointed out that the SFRs obtained from f_{24} via the relations of Rieke et al. (2009) tend to underestimate the true SFRs in $\sim 40\%$ of the cluster galaxies. We note however that no such discrepancy exists for field galaxies (Rex et al. 2010), or at least not for $z < 0.5$ (Lee et al. 2010).

Lee et al. (2010) found a trend of decreasing f_{160}/f_{24} with f_{24} , and a less pronounced trend of f_{70}/f_{24} vs. f_{24} . They attributed these trends to an increasing AGN contribution to the IR luminosities of galaxies with higher 24 μm flux densities. For our sample, there is an anti-correlation between f_{70}/f_{24} and f_{24} (see Fig. 8), even stronger than the one observed by Lee et al. (2010).

This anti-correlation may however be entirely spurious. It may originate from an increasing scatter in the f_{70}/f_{24} galaxy colors with decreasing f_{24} , combined with the sensitivity limits of our surveys (see dotted and dot-dashed lines in Fig. 8). A similar, albeit smaller, effect might explain at least part of the anti-correlation seen by Lee et al. (2010). As for their interpretation of the anti-correlation, we note that the galaxies with AGNs do not occupy a special place in our f_{70}/f_{24} vs. f_{24} diagram (red X's in Fig. 8). Clearer insight into this issue will however come from our future analysis of the spectral properties of the A1763 supercluster galaxies (paper in preparation).

2.4. Stellar masses

To determine the galaxy stellar masses, M_* , we fit the SEDs of the 467 supercluster members with the (purely stellar) model templates of Maraston (2005), adopting the Kroupa (2001) initial mass function and solar metallicity. We consider only the short-wavelength parts of the SEDs (rest-frame wavelength $\lambda \leq 4 \mu\text{m}$), and allow for dust extinction by modifying the template SEDs according to the extinction law of Calzetti et al. (2000), with $E(B - V)$ a parameter free to vary between 0 and 1 (Fontana et al. 2004). On average, we find that $E(B - V) = 0.44$ with a dispersion of 0.42.

The resulting supercluster galaxy stellar masses are correlated with the galaxy colors (see Fig. 9, top panel). The correlation suggests a physical relation between the ages of galaxy stellar populations and galaxy masses. ETGs have both high M_* and red colors. The scatter in the correlation must be largely intrinsic as it is not different for galaxies with different values of $E(B - V)$.

The galaxy stellar masses M_* are used to determine the galaxy specific star formation rates sSFRs ($\text{sSFR} \equiv \text{SFR}/M_*$). In the bottom panel of Fig. 9, we display the anti-correlation between M_* and sSFR in our sample of spectroscopically confirmed supercluster members, AGNs excluded. The slope of the correlation is close to -1 , which is indicative of an almost flat $M_*\text{-}L_{\text{IR}}$ relation. SBGs have a higher sSFR per given M_* , relative to other galaxies. This was also found by Chung et al. (2010) in their study of the Bullet cluster. In addition, the slope of their sSFR- M_* relation is very similar to ours, while Oliver et al. (2010) found a much flatter relation using a sample of galaxies from the Spitzer Wide-area InfraRed Extragalactic Legacy Survey. This difference is probably related to the way the different samples were selected, that of Oliver et al. (2010) being closer to a M_* -selected sample, while our sample is selected on the basis of the $24 \mu\text{m}$ flux density. The dashed line in Fig. 9 represents the average expected relation between sSFR and M_* for a $24 \mu\text{m}$ source of 0.2 mJy flux density, corresponding to the limit below which our sample becomes severely incomplete. This relation has been obtained using the relation of Lee et al. (2010) between f_{24} and L_{IR} at the average redshift of the A1763 supercluster, and the Kennicutt (1998) relation. Very few sources lie below the sSFR- M_* relation for an $f_{24} = 0.2$ mJy source, suggesting that the steeper slope we find for the global sSFR- M_* is indeed due to the flux-density limit in our sample.

3. Infrared luminosity functions

3.1. Completeness and purity corrections

The determination of the A1763 supercluster IR LF requires the estimations of the completeness and purity of our sample. We evaluate three types of completeness and purity corrections, the

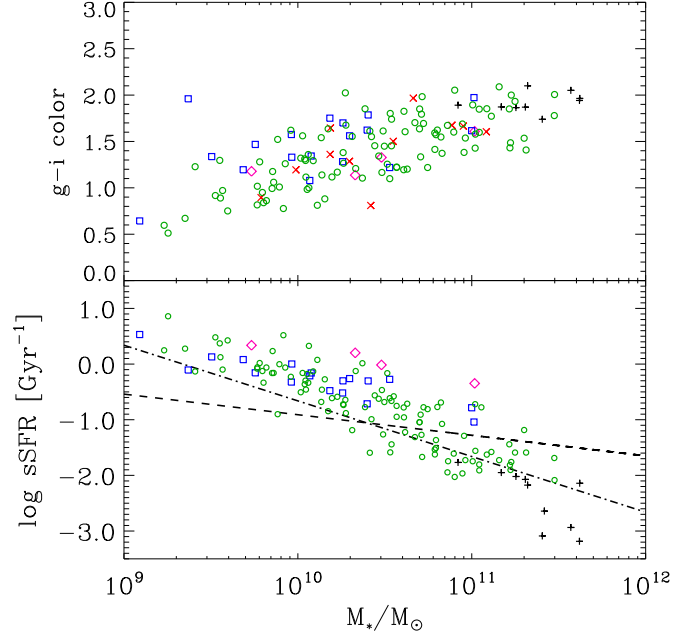


Fig. 9. *Top:* The $g - i$ color vs. stellar mass for the z sample (the spectroscopically confirmed supercluster members). *Bottom:* $\log \text{sSFR}$ vs. M_* for the same z sample, AGNs excluded. The dash-dotted line represent the expected sSFR vs. M_* relation for a $24 \mu\text{m}$ source of 0.2 mJy flux density (i.e. at the completeness limit of our Spitzer survey), obtained using the relations of Lee et al. (2010) and Kennicutt (1998). The dashed line is the relation of Oliver et al. (2010) for galaxies from the Spitzer Wide-area InfraRed Extragalactic Legacy Survey in the redshift range $0.2 < z < 0.3$. In both panels, symbols have the same meaning as in Fig. 6.

first for the source detection, the second for the (spectroscopic or photometric) redshift determination, the third for the membership assignment.

In the first step, we need to consider the completeness and purity of the detected $24 \mu\text{m}$ sources in the photometric catalog, and we model these corrections following Fadda et al. (2006, see Sect. 2). We fit a third order polynomial to the completeness function of Fadda et al. (2006) to determine the completeness correction

$$C_{\text{det}} = 1 + 0.04x + 0.36x^2 + 0.97x^3, \quad (1)$$

for $x \equiv \log f_{24}[\text{mJy}] \leq 0$, and $C_{\text{det}} = 1$ for $x > 0$. The purity was approximated by a constant, $P_{\text{det}} \sim 0.95$ at all flux levels.

In the second step, we consider the completeness of the sample of sources for which we could establish the cluster membership, i.e. the sample of sources with either a spectroscopic redshift (z) or a photometric redshift (z_p) estimate. We call $N_{z \cup p}$ the number of sources with either z or z_p , and N the total number of sources in the $24 \mu\text{m}$ catalog. The completeness of the sample of sources with either a z or z_p estimate is given by $C_{z \cup p} \equiv N_{z \cup p}/N$, as a function of f_{24} .

In the third step, we estimate the completeness and purity of the sample of selected cluster members (467 in total, see Sect. 2.2) based on their z or z_p . Since the membership assignment is imperfect, we need a purity correction to account for the

erroneous membership assignments, and a completeness correction to account for those real members that have not been selected.

We first evaluate the membership corrections for the spectroscopic sample. The fraction of galaxies incorrectly assigned to the cluster on the basis of their z cannot be directly determined from the data. On the basis of the analyses of cluster-sized halos extracted from cosmological simulations (Biviano et al. 2006; Wojtak et al. 2007; Mamon et al. 2010), we assume a membership purity $P_{zm} = 0.8$ and no completeness correction for the sample of spectroscopic members.

We then consider the corrections to be applied to the sample of galaxies without available z , whose membership can only be established from their z_p . We proceed in a way similar to that adopted in Sect. 2.2 except that now the z_p -range for membership selection is fixed to the values previously determined, $0.166 \leq z_p \leq 0.290$. As in Sect. 2.2, we have to determine the completeness and purity by considering galaxies with z that would qualify as members based on their z_p , $N_{pm \cap z}$. A subset of the galaxies in this subsample, $N_{pm \cap zm}$, are spectroscopic members. We therefore define the membership purity of the sample of N_{pm} galaxies as the fraction $P_{pm} \equiv N_{pm \cap zm}/N_{pm \cap z}$ as a function of f_{24} . Among the $N_{zm \cap p}$ z -selected members that also have z_p estimates, there are $N_{pm \cap zm}$ that would also be identified as members based on their z_p . The membership completeness of the sample of z_p -selected members is therefore given by $C_{pm} \equiv N_{pm \cap zm}/N_{zm \cap p}$ as a function of f_{24} .

We define N_{zm} to be the number of galaxies defined to be cluster members based on their z , and N_{pm} the number of galaxies defined to be supercluster members based on their z_p . The corrected number of members is

$$N_c \equiv \frac{P_{det}}{C_{det}} \cdot \frac{1}{C_{z \cup p}} \cdot (P_{zm} \cdot N_{zm} + \frac{P_{pm}}{C_{pm}} \cdot N_{pm}). \quad (2)$$

By combining the data for galaxies with available z_p with those for galaxies with available z , we obtain a larger sample of members, but at the expense of a larger uncertainty in the membership assignments. The resulting sample (the $z \cup z_p$ sample) is therefore more complete, but less pure than the sample of supercluster members constructed using only galaxies with available z (the z sample). To check for possible systematics related to our purity corrections, we also determine the IR LF for the z sample. We call N_z the number of galaxies with available z among the total of 24 μm -selected sources. The completeness of this spectroscopic sample is $C_z \equiv N_z/N$. Therefore, the corrected number of members of the z sample is

$$N_{cz} \equiv \frac{P_{det}}{C_{det}} \cdot \frac{1}{C_z} \cdot P_{zm} \cdot N_{zm}. \quad (3)$$

We note that in eqs. 2, 3 we have omitted the explicit f_{24} -dependence of the individual terms to simplify the notation.

3.2. The supercluster luminosity function

We determine the IR LF of the supercluster by counting the galaxies in (logarithmic) luminosity bins, and weighting the counts by the correction functions described above (Sect. 3.1; the same procedure was used by Rujopakarn et al. 2010). Since the correction factor becomes very high at low fluxes, we only consider galaxies with $f_{24} \geq 0.2$ mJy (317 out of the originally selected 467 cluster members, 124 selected as members on the basis of their z). We multiply the counts by the fractions of non-AGN galaxies in each L_{IR} -bin (see Fig. 5) to remove the AGN contribution from the IR LF.

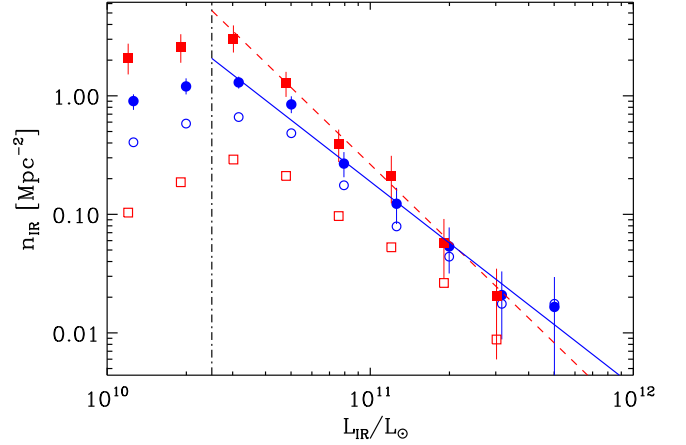


Fig. 10. The IR LF of A1763. Filled and empty symbols represent the counts after and, respectively, before purity and completeness corrections. Counts have been multiplied by the fractions of non-AGN galaxies in each L_{IR} -bin (see Fig. 5) to remove the AGN contribution from the IR LF. Blue dots (respectively, red squares) represent the counts based on the $z \cup z_p$ (respectively, z) sample. 1σ error bars based on 100 bootstrap re-samplings are shown. The square symbols have been displaced by -0.02 in $\log L_{IR}$ for clarity. The vertical dash-dotted line indicates the L_{IR} lower limit ($L_{IR}/L_{\odot} = 2.5 \cdot 10^{10}$) that corresponds to the 0.2 mJy flux density limit adopted for the determination of the IR LF. The solid blue (respectively dashed red) line represents the power-law best-fit to the IR LF represented by the blue filled dots (respectively, red squares) with $L_{IR}/L_{\odot} \geq 2.5 \cdot 10^{10}$.

We obtain two determinations of the IR LF by using in one case the $z \cup z_p$ sample, and in the other case the z sample (see Sect. 2.2). The error bars of the IR LF are estimated with a bootstrap re-sampling technique (Efron & Tibshirani 1986). Both the galaxy counts and the correction functions are computed for each bootstrap re-sampling.

The resulting IR LF determinations are shown in Fig. 10. Filled symbols represent the corrected counts, open symbols the uncorrected counts, and the ratios of the two give the correction factors applied (based on eqs. 2 and 3 for the $z \cup z_p$ and z sample, respectively). The two determinations agree within the error bars down to $L_{IR}/L_{\odot} \approx 4 \cdot 10^{10}$; at lower L_{IR} the correction factor for the counts in the z sample is very large (> 10), and therefore rather uncertain. The agreement of the two IR LF determinations down to $L_{IR}/L_{\odot} \approx 4 \cdot 10^{10}$ suggests that the completeness and purity corrections that we have applied to the two subsamples are reasonably accurate.

The vertical dash-dotted line in Fig. 10 indicates the L_{IR} lower limit corresponding to the adopted limit of $f_{24} = 0.2$ mJy for the IR LF determination, $L_{IR} \approx 2.5 \cdot 10^{10} L_{\odot}$ (see Fig. 7; this limit is not very precise because of the dispersion in the L_{IR} - f_{24} relation).

We try fitting the IR LF at $L_{IR} \geq 2.5 \cdot 10^{10} L_{\odot}$ with a Schechter (1976) function, but the best-fit parameters are poorly constrained. This is mostly because the Schechter function decreases steeply at high luminosities, beyond L_{IR}^* , while our IR LF does not show a change in slope over the full range of luminosities. Some authors have advocated the use of a double power-law as a fitting function for IR LFs (Babbedge et al. 2006;

Table 1. Slope parameters from power-law fits to the IR LFs

Sample	Region	α	χ^2	dof
$z \cup z_p$	Whole	-1.7 ± 0.1	3.3	6
$z \cup z_p$	Core	-2.2 ± 0.7	0.5	4
$z \cup z_p$	Filament	-1.5 ± 0.3	3.1	5
$z \cup z_p$	Outskirts	-2.4 ± 0.4	8.8	6
z	Whole	-2.1 ± 0.5	0.6	5
z	Core	-1.8 ± 0.6	0.1	3
z	Filament	-1.8 ± 0.3	1.6	5
z	Outskirts	-2.2 ± 0.9	0.2	3

Goto et al. 2011). The characteristic luminosity at which the IR LF of field galaxies changes slope in this case is $\sim 5 \times 10^{10} L_\odot$ (Goto et al. 2011), which is close to our adopted completeness limit. A single power-law function can thus be expected to provide a good fit to our IR LF over the full range of luminosities down to the completeness limit. This is indeed the case, as shown in Fig. 10, where the solid and dash-dotted lines represent the best-fit power-law functions for the two samples. The best-fit values of the slope parameter are given in Table 1 (region ‘Whole’); the quality of the fits, as indicated by the listed χ^2 values, is good, and indicates that a two-parameter fit (e.g. with a Schechter function) is not required (note that the χ^2 values are *not* reduced χ^2). The values we obtain for the two samples are compatible within the 1- σ error bars.

3.3. Environmental dependence

To investigate possible environmental effects on the IR LF, we consider three different regions of the A1763 supercluster. To more clearly define the location of the large-scale filament identified in Paper 0, we determine the galaxy density map of the supercluster, as traced by IR-emitting, star-forming galaxies, by running an adaptive-kernel technique (see, e.g., Biviano et al. 1996) on the sample of 432 non-AGN supercluster members (see Sect. 2.2 and 2.3). We consider only the $z \cup z_p$ sample in this case, because it is more complete than the z sample, and completeness is more important than purity when determining the density map, as long as there are no contaminating background or foreground structures in the sample (and we think there are not, see Sect. 2.2).

The result is shown in Fig. 11. A clear over-density of galaxies is seen extending to the north-east direction from the central cluster region⁵. This region coincides with the filamentary structure(s) found in Paper 0. We draw two almost parallel lines delimiting this over-density region in order to identify the “filament” region. We clearly define the “filament” region by excluding the “core” region, which we define to be the 1.34 Mpc circular region centered on the A1763 cluster center. This region corresponds to the projection of the sphere with a mass over-density 500 times the critical density, and its radius is estimated as $r_{500} = 0.65 r_{200}$, using the mass profile of Navarro et al. (1997) with a concentration parameter $c = 4$, typical of massive galaxy clusters (e.g. Katgert et al. 2004). We finally de-

⁵ Follow-up spectroscopic observations show that this galaxy over-density continues beyond the region covered by our Spitzer observations. The apparent cut-off of the filamentary structure visible at the edge of the Spitzer field in Fig. 11 is an edge-effect of the adaptive-kernel algorithm.

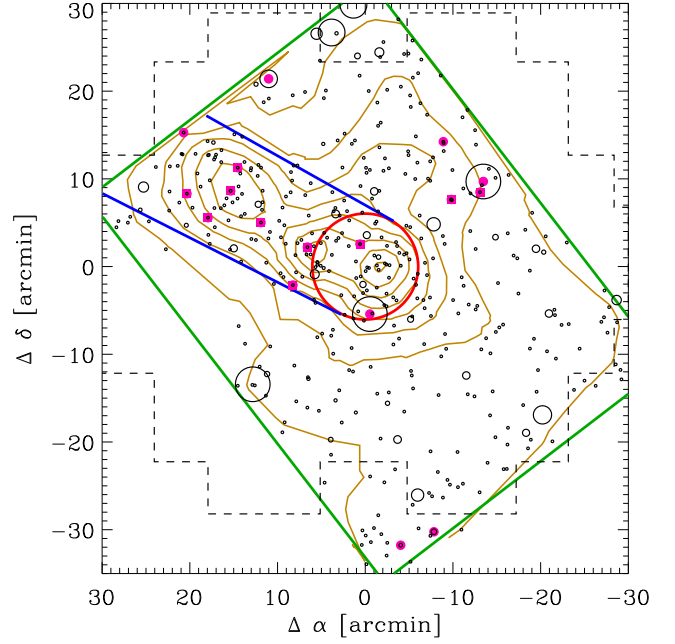


Fig. 11. Diagram illustrating the three mutually exclusive regions for which independent IR LFs have been defined. The red circle defines the “core” region, which is centered on the cluster A1763 and extends to a radius $r_{500} = 1.34$ Mpc. The two almost parallel blue segments delimit the extended over-density of supercluster members outside the core, which we identify with the large-scale “filament” region, discovered in Paper 0. The “outskirts” region is delimited by the green parallelogram, which represents the extent of the $24 \mu\text{m}$ observations, excluding the core and filament regions. We also show the region corresponding to the Palomar r -band observations (connected dashed black segments). The (brown) contours are isocontours of galaxy number density, linearly spaced, obtained by running an adaptive-kernel technique on the spatial distribution of the 432 non-AGN, IR-emitting supercluster members of the $z \cup z_p$ sample. Positions of these galaxies are indicated by the (black) circles, with sizes proportional to the galaxy sSFRs. Filled (pink) symbols mark the positions of the LIRGs in the $z \cup z_p$ sample, squares for spectroscopically confirmed members, dots for members selected on the basis of their z_p .

fine the “outskirts” region as the remaining part of the observed $24 \mu\text{m}$ survey region, excluding the core and the filament.

The IR LFs of the three different regions were determined as described in Sect. 3.1, using completeness and purity corrections that are appropriate for each considered region, and multiplying the counts by the fractions of non-AGN galaxies in each L_{IR} -bin and each region to remove the AGN contribution from the IR LFs. Error bars were determined via a bootstrap re-sampling procedure. The three IR LFs are displayed in the left-hand panels of Fig. 12, for both the $z \cup z_p$ (top panel) and the z sample (bottom panel). Power-law function fits to the three IR LFs are shown as dashed lines, and the best-fitting values of the slope parameter are given in Table 1.

The slopes of the three region IR LFs do not differ significantly, but taken at face value they suggest that the filament has a flatter IR LF than both the outskirts and (for the $z \cup z_p$ sample) the core. The IR LF of the filament region is flatter because

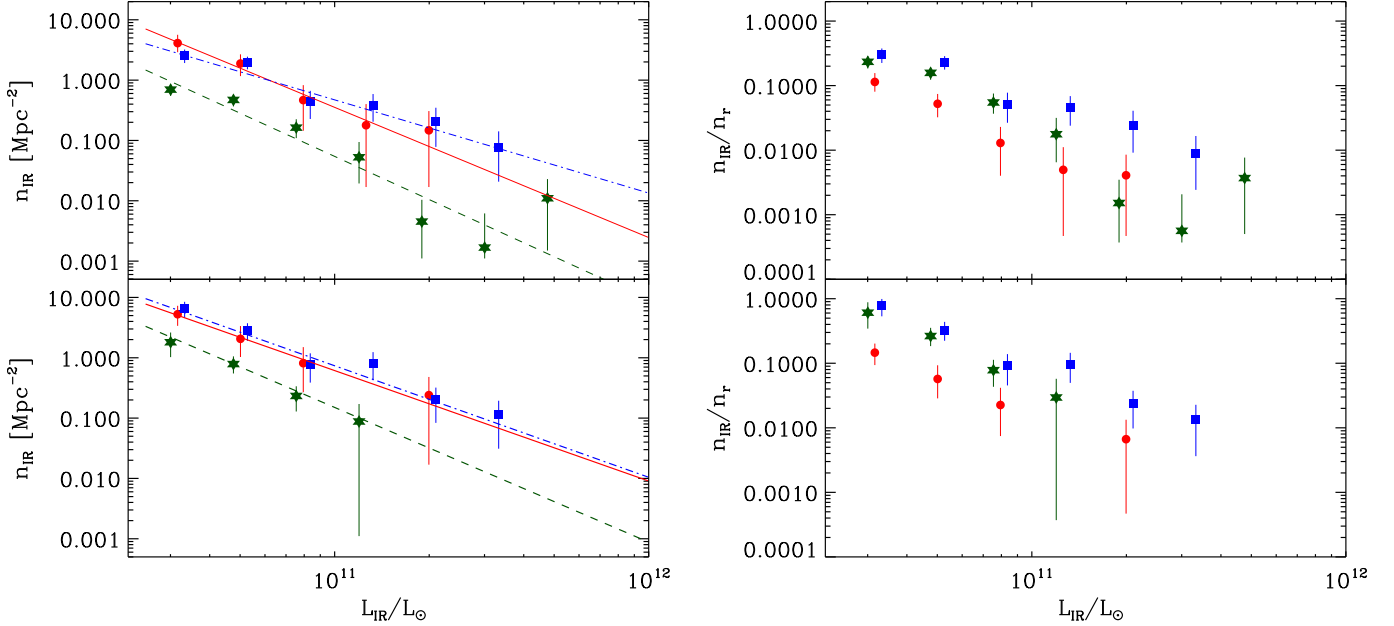


Fig. 12. The IR LFs of three different regions in the A1763 supercluster: core (red dots), filament (blue squares), and outskirts (green stars). 1σ error bars based on 100 bootstrap re-samplings are shown. All IR LFs are corrected for purity and completeness in the corresponding regions. Counts have been multiplied by the fractions of non-AGN galaxies in each L_{IR} -bin and in each region to remove the AGN contribution from the IR LFs. The IR LFs of the upper (respectively, lower) panels have been obtained using the $z \cup z_p$ sample (respectively, z sample) of supercluster members. *Left panels* show the number densities of IR-emitting galaxies. Lines represent the best-fit power-law functions to the IR LFs. In the *right panels*, the number densities of IR galaxies have been normalized by the average number densities of galaxies with a r -band luminosity $\geq 7 \cdot 10^9 L_{\odot}$ within each region.

of an excess of LIRGs relative to the other regions. This is also apparent from a visual inspection of Fig. 12 and also of Fig. 11, where we show the spatial positions of all supercluster members in the $z \cup z_p$ sample and indicate the LIRGs with pink symbols (square symbols for LIRGs of the z sample).

Fig. 12 (left panels) also shows that at lower L_{IR} , the number densities of IR-emitting galaxies are similar in the core and in the filament regions, and lowest in the outskirts region. When considering the implications of this comparison, one must take into account that the three selected regions are characterized by different densities of normal galaxies, highest in the core, lowest in the outskirts. Similarities in the IR LFs of different regions could be caused by a combination of different densities of normal galaxies and different fractions of IR-emitting galaxies among the total. Viceversa, different IR LFs could simply reflect differences in the densities of normal galaxies combined with similar IR-emitting galaxy fractions among the total.

It is therefore also important to compare the relative fractions of IR-emitting galaxies in the different regions. For this, we must determine the densities of normal galaxies in the three different regions. By adopting the same methodology used for a derivation of the IR LF (see Sect. 3.1), we determine the r -band LFs in the three regions. These LFs are well fitted by Schechter functions, and their shapes are not statistically different according to a χ^2 test (DeGroot 1987). We then integrate these LFs to derive the number densities of r -band selected galaxies with r -band luminosity⁶ $L_r \geq 7 \cdot 10^9 L_{\odot}$. This luminosity represents the

lower limit above which our determinations of the r -band LFs appear to be robust, i.e. independent of sample choice (the $z \cup z_p$ sample or the z sample). It corresponds to a stellar mass $M_{\star} \approx 6\text{--}7 \cdot 10^9 M_{\odot}$ (Bell et al. 2003; Bernardi et al. 2010), which roughly matches the lower stellar mass limit of the IR detected galaxy population in A1763 (see Fig. 9).

The r -band number densities (n_r) are given in Table 2. The number density of r -band selected galaxies in the filament is in-between those of the core and the outskirts, as expected.

We divide the IR LFs of the three regions by their n_r to produce the plots shown in the right-hand panels of Fig. 12 (top panel: $z \cup z_p$ sample; bottom panel: z sample). When scaled by the relative densities of r -band selected cluster members in the different regions, the filament displays the highest over-density of IR-emitting galaxies, with respect to both the core and the outskirts, at all L_{IR} . According to a χ^2 test (DeGroot 1987), the difference is very significant with respect to the core (99.9 % significance level for both the $z \cup z_p$ and the z sample), but not significant with respect to the outskirts. The global difference between the outskirts and the core IR LFs is marginally significant (98 % significance level for both the $z \cup z_p$ and the z sample).

The difference between the IR LFs in the three supercluster regions reflects a different SFR per galaxy. By integrating the IR LF down to our adopted completeness limit, we obtain the total L_{IR} of galaxies in the three regions, which we then convert to a total SFR (ΣSFR hereafter) via the relation of Kennicutt

⁶ Because of the similar shapes of the r -band LFs of the three regions, the exact choice of the luminosity limit for the integration of the r -

band LFs does not strongly affect the relative ratios of the three regions number densities ($\leq \pm 10\%$ when the luminosity limit is increased by up to a factor three).

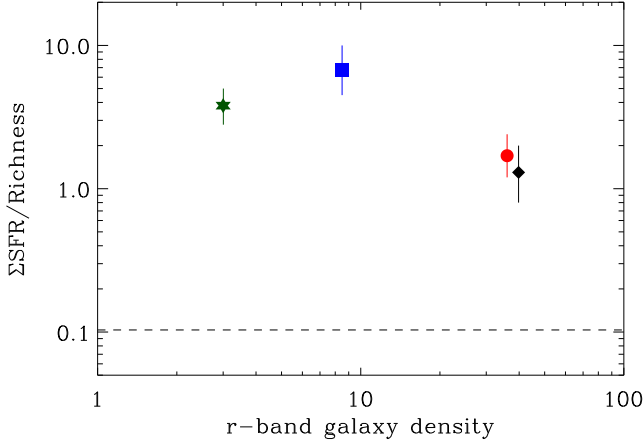


Fig. 13. $\Sigma\text{SFR}/\text{richness}$ (in units of $M_{\odot} \text{ yr}^{-1}$) as a function of the average r -band galaxy density within each region. Richnesses and densities are estimated using galaxies brighter than $7 \times 10^9 L_{\odot}$ in the r -band. Different symbols identify the three different regions, as in Fig. 12, and the filled black diamond identifies the region within $R \leq 0.5 r_{200}$. 1σ error bars are shown. The dashed line represents the expected value at the cluster mean z , using the relation of Bai et al. (2009) between $\Sigma\text{SFR}/\text{mass}$ and z , and the richness/mass value of the A1763 virial ($R \leq r_{200}$) region (see Sect. 3.4).

Table 2. Properties of different supercluster regions. ΣSFR is the total SFR of IR-emitting galaxies. $\Sigma\text{SFR}/M_{200}$ is the ΣSFR normalized by the total gravitational cluster mass.

Property	core	Supercluster regions		
		filament	outskirts	$R \leq 0.5 r_{200}$
Area [Mpc ²]	5.9	17.4	90.4	3.6
n_r [Mpc ⁻²]	36.0 ± 6.7	8.5 ± 1.8	3.0 ± 0.4	39.8 ± 7.3
$\Sigma\text{SFR}/(\text{Area} \cdot n_r)$ [$M_{\star} \text{ yr}^{-1}$]	$1.7^{+0.7}_{-0.5}$	$6.7^{+3.3}_{-2.2}$	$3.8^{+1.2}_{-1.0}$	$1.3^{+0.7}_{-0.5}$
$\Sigma\text{SFR}/M_{200}$ [$M_{\odot} \text{ yr}^{-1}/10^{14} M_{\odot}$]				26^{+11}_{-9}

(1998). We divide the ΣSFR values of the three regions by the areas of the three regions and the number densities of r -band selected galaxies in the three regions to obtain the average SFRs per r -band selected galaxy in each region⁷. The values are given in Table 2 for the $z \cup z_p$ sample (consistent values are found for the z sample, within the errors); they are displayed as a function of the average density of r -band selected galaxies in Fig. 13. The average SFR is highest for the filament region, intermediate for the outskirts region, and lowest for the core region. The difference between the filament and the core values is significant at

⁷ These averages are clearly not representative of the typical galaxy SFR, as they are biased high by the high SFRs in the (relatively few) very bright IR emitting galaxies.

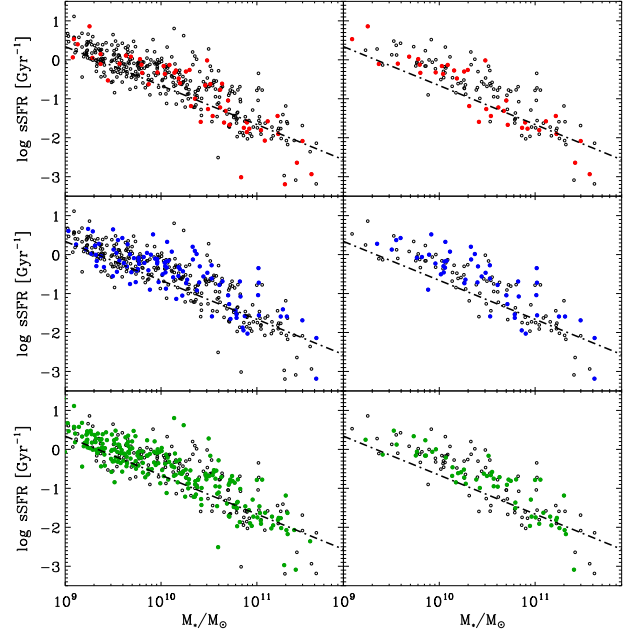


Fig. 14. Galaxy $s\text{SFR}$ vs. M_{\star} in three different regions of the A1763 supercluster. Open (black) circles represent all non-AGN, IR-emitting supercluster members. Filled dots identify supercluster members in the core region (red dots, top panels), in the filament region (blue dots, middle panels), in the outskirts region (green dots, bottom panels). The panels on the left are based on the $z \cup z_p$ sample, those on the right on the z sample. The dash-dotted line has the same meaning as in Fig. 9.

slightly more than 2σ , i.e. at the 98 % confidence level for a Gaussian distribution of errors, that between the core and the outskirts values is significant at the 96 % confidence level, and that between the outskirts and the filament values is not significant (< 90 % confidence level).

Are the excess LIRGs in the filament region massive galaxies or low-mass galaxies with high levels of $s\text{SFR}$ s? To understand this issue, in Fig. 11 we use symbol sizes proportional to the galaxy $s\text{SFR}$ s to represent the spatial positions of the 432 non-AGN supercluster members. Most of the LIRGs have rather low $s\text{SFR}$ s, meaning that they have both high L_{IR} and high M_{\star} .

Another way to look at this issue is to compare the bi-dimensional distributions of galaxies in different regions in a $s\text{SFR}$ vs. M_{\star} diagram, shown in Fig. 14 for both the $z \cup z_p$ and z sample (left- and right-hand panels, respectively). Galaxies of different regions of the superclusters appear to have similar $s\text{SFR}-M_{\star}$ distributions. A statistical assessment of this result is obtained by comparing the $s\text{SFR}-M_{\star}$ distributions two by two via bi-dimensional Kolmogorov-Smirnov tests (Peacock 1983; Fasano & Franceschini 1987), under the null hypothesis that the distributions are drawn from the same parent one. Only in one case, core vs. outskirts, and only for the $z \cup z_p$ sample we do find that the null hypothesis is rejected, but only with marginal significance (97 % confidence level).

The similarity between the different $s\text{SFR}-M_{\star}$ distributions suggests that similar modes of star formation take place in galaxies in different environments. This similarity has been noted before in different data sets (Peng et al. 2010). Additional support for this result comes from the analysis of the fractions of IR su-

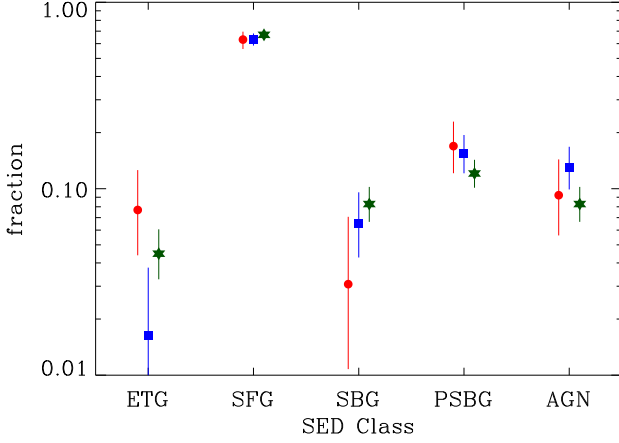


Fig. 15. The fractions of IR supercluster members ($z \cup z_p$ sample) in different SED classes in the three different environments. Different symbols identify the three different regions, as in Fig. 12.

percluster members in different SED classes. These fractions are displayed in Fig. 15 for the different regions of the supercluster (results are displayed for the $z \cup z_p$ sample; very similar results are found for the z sample, and are not shown here). They are clearly very similar, except perhaps for a very marginal excess of ETGs in the core region. The fraction of AGNs among IR-emitting galaxies is similar to that found in Paper 2 and in other galaxy clusters (e.g. Geach et al. 2009; Krick et al. 2009; Chung et al. 2010).

3.4. Comparison with previous results

We compare the IR LF of A1763 with those of Bai et al. (2009), Tran et al. (2009), and Chung et al. (2010), for which the parameters of the best-fit Schechter function are available. Ideally, one would like to compare IR LFs obtained within regions of similar galaxy number densities, to highlight differences due to different fractions of IR-emitting galaxies. Since previous determinations have been limited to the inner, virialized cluster regions, we consider in this comparison only the IR LF of the core region of A1763.

The areas where the LFs of Bai et al. (2009), Tran et al. (2009), Chung et al. (2010), and the A1763 core have been derived correspond to circular regions of effective limiting radii 0.90, 0.74, 0.82, and 0.65, in units of the respective cluster r_{200} . We derive the virial radii of the clusters from their velocity dispersions (taken from Biviano et al. 1996; Quintana et al. 1996; Fisher et al. 1998; Barrena et al. 2002) via the relation of Mauduit & Mamon (2007, Appendix A). The effective limiting radii of the four clusters are similar, but not identical. We therefore apply scaling factors to the cluster IR LFs proportional to the estimated number densities of normal galaxies within these limiting radii. We compute these projected densities as in Appendix B.2 of Mamon et al. (2010), using the individual cluster virial radii and the model profile of Navarro et al. (1997) with concentration $c \simeq 3$ (a typical value for rich clusters; see, e.g. Biviano & Poggianti 2009). Setting to unity the scaling factor for the IR LF of the A1763 core, the other scaling factors are

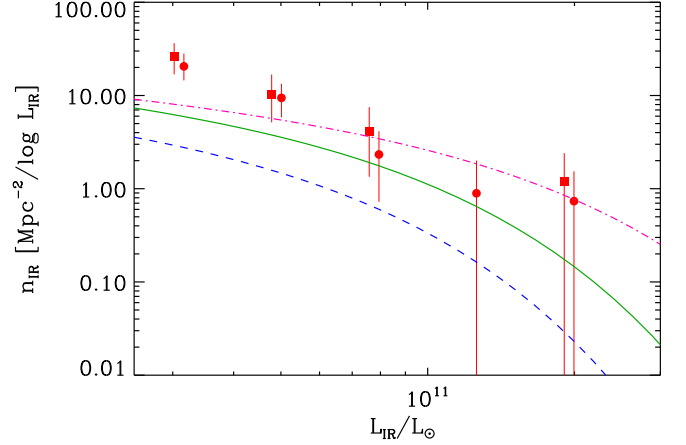


Fig. 16. The IR LF of the A1763 core region (same as in Fig. 12; filled red dots: $z \cup z_p$ sample; filled red squares – slightly displaced along the x-axis for clarity – : z -only sample; 1σ error bars), compared to the best-fit Schechter IR LF of Bai et al. (2009, solid green curve), Chung et al. (2010, dash-dotted pink curve), and Tran et al. (2009, dashed blue curve). Note that the Schechter IR LFs have been corrected to take into account the different survey areas and the different cluster redshifts, as described in the text.

1.40, 1.14, and 1.27, for the LF of Bai et al. (2009), Tran et al. (2009), and Chung et al. (2010), respectively.

In addition to the density correction, since the different clusters are located at different redshifts, we rescale the best-fit Schechter parameters obtained for these clusters to the redshift of A1763, adopting the evolution relation of Bai et al. (2009). The result is shown in Fig. 16. We note that to compare the different luminosity functions, we divide the number densities of the A1763 core IR LF by the logarithmic interval we used for the binning, 0.2.

The IR LF of the A1763 core lies significantly above all other IR LFs at the faint end, while it is consistent with them at the bright end. It is most similar to the IR LF established by Chung et al. (2010) for the Bullet cluster. There clearly seems to be a large variance in the cluster IR LFs, even after correcting for evolutionary effects and after rescaling for the different galaxy densities in the cluster areas sampled by the different surveys. Part of the variance is caused by observational errors, and the IR LF of Tran et al. (2009), which appears to lie below that of Bai et al. (2009) in Fig. 16, is consistent with it within the uncertainties (see Fig. 7 in Tran et al. 2009). As a source of intrinsic variance, one could consider the effect of an increasing fraction of IR-emitting galaxies with clustercentric radius (e.g. Bai et al. 2009; Haines et al. 2009a). However, this trend is far too small to account for the variance we see in the IR LFs, given that they were obtained within rather similar limiting effective radii. Moreover, among the four LFs displayed in Fig. 16, that of the A1763 core has been determined within the smallest effective radius, and yet it appears to lie above all the others.

Another way of comparing IR LFs for clusters of different masses and at different redshifts is to look at the variation in the total cluster SFR within a fixed aperture – in units of r_{200} – normalized by the cluster total mass, M_{200} (Geach et al. 2006; Bai et al. 2009; Chung et al. 2010). The mass of the virial region of A1763, $M_{200} = 9.9 \times 10^{14} M_{\odot}$, is obtained from the values of

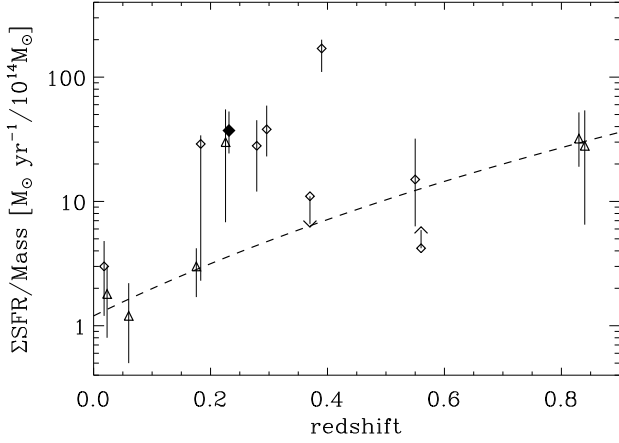


Fig. 17. $\Sigma\text{SFR}/M_{200}$ (in units of $M_{\odot} \text{ yr}^{-1} / 10^{14} M_{\odot}$), where ΣSFR is estimated within a region of radius $0.5 r_{200}$, as a function of redshift for A1763 (filled diamond) and for other clusters from the literature. Triangles and open diamonds denote values taken from Bai et al. (2009) and Chung et al. (2010), respectively. 1σ error bars are shown. The downward-directed (respectively upward-directed) arrow denotes an upper (respectively lower) limit. The curve represents the fitting relation of Bai et al. (2009) $\Sigma\text{SFR}/\text{mass} = 1.2(1+z)^{5.3}$.

r_{200} and v_{200} (see Sect. 3.3). The estimate is based on 357 member galaxies (see Sect. 2.2). According to Biviano et al. (2006), a mass estimate based on a galaxy sample of this size has an uncertainty of $\approx 25\%$.

Following Bai et al. (2007, 2009), we evaluate ΣSFR within $R \leq 0.5 r_{200}$ and normalize it by the global cluster mass M_{200} . The value is reported in Table 2. The quoted error includes the contribution from both the ΣSFR uncertainty (estimated via a bootstrap procedure) and the mass uncertainty, the latter being the main source of error. To compare it with the determinations of Bai et al. (2007) we need to apply a correction to account for the different L_{IR} limit of our IR LF ($2.5 \cdot 10^{10} L_{\odot}$) and that of Bai et al. (2007) ($1.2 \cdot 10^{10} L_{\odot}$). Using the IR LF of Bai et al. (2009) evolved to the mean redshift of A1763, we estimate a correction factor of 1.4. We plot the corrected value for the A1763 $0.5 r_{200}$ region in Fig. 17 together with the values for other clusters taken from the literature (Geach et al. 2006; Bai et al. 2009; Chung et al. 2010) and based on *IRAS* (Meusinger et al. 2000), *ISO* (Fadda et al. 2000; Duc et al. 2002; Metcalfe et al. 2003; Biviano et al. 2004; Duc et al. 2004; Coia et al. 2005b), and *Spitzer* (Geach et al. 2006; Bai et al. 2006, 2007, 2009; Haines et al. 2009b; Chung et al. 2010) data. The value for A1763 lies in the same locus of the diagram as other clusters at similar redshifts. There is a trend of increasing $\Sigma\text{SFR}/\text{mass}$ with redshift, a sort of IR Butcher-Oemler effect (Butcher & Oemler 1984; Saintonge et al. 2008; Haines et al. 2009a; Tempurin et al. 2009). This trend has been noticed before and modeled with a power-law relation in $(1+z)$ by Geach et al. (2006) and Bai et al. (2009), mimicking the trend found by Cowie et al. (2004) for the number of ultra-LIRG radio sources in the field, or the trend found by Kodama et al. (2004) for the ΣSFR of cluster galaxies, based on optical-line spectroscopic estimates of the galaxy SFRs. The best-fit relation obtained by Bai et al. (2009) is shown in Fig. 17. It clearly fails to fit the data in the z -range 0.2–0.4.

The quantity $\Sigma\text{SFR}/\text{mass}$ appears to evolve rapidly from $z \approx 0.4$ to 0, while it remains almost constant for $z \gtrsim 0.4$.

To explore the environmental dependence of the mass-normalized SFR, we would need to determine the masses of the filament and outskirts regions, but this is not possible since these regions do not correspond to virialized, collapsed structures. With the A1763 mass M_{200} and r -band richness within r_{200} , we define a mass-to-richness ratio that we use to determine $\Sigma\text{SFR}/\text{richness}$ at the average redshift of A1763 from the evolutionary relation of Bai et al. (2009). This is displayed in Fig. 13 with a dashed line and allows an indirect comparison of Fig. 17 with Fig. 13, where we show the $\Sigma\text{SFR}/\text{richness}$ of the $R \leq 0.5 r_{200}$ region and also of the core, filament, and outskirts regions (see Sect. 3.3). We can summarize the results illustrated in Figs. 17 and 13 by saying that the SFR per galaxy increases with z in clusters, and it is not a monotonic function of the density of the environment.

4. Discussion

Our analysis of the IR LF of the A1763 supercluster has confirmed our findings of Paper 0, namely the filament is the most probable site of galaxy star formation. We have shown that the IR LF of filament galaxies lies above those of the core and the outskirts, when these three IR LFs are normalized by the average densities of normal, r -band selected, galaxies in the three regions (Fig. 12, right panels). In other words, filament galaxies have a higher chance of being IR-emitting than both core and outskirts galaxies. Since we have corrected the IR LFs for the contribution of galaxies with AGNs, the excess fraction of IR galaxies in the filament can also be read as an excess fraction of star-forming galaxies⁸. The result of our analysis extends the original finding of Paper 0 by showing that there is an excess fraction of star-forming galaxies in the filament relative to other supercluster regions, at all levels of star-formation down to our L_{IR} completeness limit, which corresponds to $\text{SFR} \approx 4 M_{\odot} \text{ yr}^{-1}$ (see Sect. 3.3).

Several authors have previously noted the increasing fraction of IR-emitting, star-forming galaxies with increasing cluster-centric distance and the lack of LIRGs in cluster cores (Bai et al. 2006, 2009; Haines et al. 2009a; Tempurin et al. 2009; Davies et al. 2010; Finn et al. 2010). Our finding indicates that the relation is not simply one of galaxy SFR with cluster-centric distance or local density (see Fig. 13). Galaxy filaments are regions of intermediate galaxy densities between cluster cores and cluster outskirts, and galaxies in the A1763 filament are not farther out from the A1763 cluster center than galaxies in the A1763 outskirts (see Fig. 11). The higher fraction of star-forming galaxies in medium-density environments has already been noted in other IR (Koyama et al. 2008; Gallazzi et al. 2009; Koyama et al. 2010) or optical (Braglia et al. 2007; Porter & Raychaudhury 2007; Boué et al. 2008; Porter et al. 2008; Braglia et al. 2009) studies of superclusters.

An interesting aspect of the higher fraction of star-forming galaxies in the A1763 filament is that these galaxies are relatively massive, with a relatively low sSFR (see Fig. 11). The sSFR- M_{\star} relation is very similar in the core, the filament, and the outskirts regions (see Fig. 14), i.e. at a given M_{\star} filament galaxies do not have enhanced sSFRs. Both the universality of the sSFR- M_{\star} relation across different environments

⁸ Had we omitted to correct the IR LFs for the presence of AGNs, the results of this paper would not have been significantly affected.

and the relatively low-sSFR of dust-reddened high-SFR galaxies in medium-density environments have been noted before (Peng et al. 2010; Gallazzi et al. 2009).

The similarity of the sSFR- M_\star relation of galaxies in different supercluster regions suggests that the regions share a similar mode of star formation. This conclusion is supported by the similarity of the SED-class distributions in the different regions (Fig. 15). About 65 % of the IR-emitting galaxies in all the supercluster regions belong to the normal SFG SED-class. Only ~ 6 % and, respectively, ~ 15 % belong to the SBG and, respectively, PSBG classes, ~ 10 % to the AGN class, and ~ 4 % (slightly more in the core) to the ETG class. These fractions indicate that, overall, the dominant mode of star formation in IR-emitting galaxies across the whole supercluster is that of normal late-type galaxies. Haines et al. (2011b) reached the same conclusion from their analysis of IR and UV data for the nearby Shapley supercluster.

Even if the SFG SED class characterizes most of the IR-emitting galaxies, the brightest of them, LIRGs, mostly belong to the SBG SED class (10 out of 18 LIRGs belong to the SBG SED class; see also Fig. 5). It is known that LIRGs are mostly powered by starbursts (e.g. da Cunha et al. 2010; Fadda et al. 2010; Finn et al. 2010), which occur as a consequence of close galaxy-galaxy interactions (e.g. Spitzer & Baade 1951; Negroponte & White 1983; Bushouse 1987; Sanders et al. 1988; Barnes 1992; Hwang et al. 2010; Teyssier et al. 2010). In A1763, LIRGs are more frequently found in the filament than in other regions of the supercluster (Fig. 11). In cluster cores, interactions are frequent but do not significantly affect the interacting galaxies because of the very high speed of these encounters (repeated fast encounters might however be relevant for dwarf galaxies, Moore et al. 1996). In filaments, on the other hand, the frequency of galaxy-galaxy interactions is still relatively high, and they occur at a relatively low speed, since the filament environment is characterized by higher galaxy densities than the field, and lower velocity dispersions than the cluster core (Paper 0). The tidal (or resonance, see D’Onghia et al. 2010) effects of galaxy-galaxy interactions are stronger when the collisions occur at small relative velocities (Mamon 1996; Makino & Hut 1997), so filaments (and poor groups) are the ideal environment for significant effects to result from galaxy-galaxy interactions. These interactions may sporadically lead to (major) mergers.

SBGs are likely to evolve into galaxies of the PSBG class. Further evolution is hard to predict. It has been argued that AGNs are a late outcome of the starburst process (e.g. Umemura et al. 1999; Emonts et al. 2006; Younger et al. 2009). In this case, we could estimate that starburst episodes are affecting, or have affected in the past ~ 1 Gyr, ~ 30 % of all the IR-emitting galaxies in the A1763. According to Wild et al. (2009), there is a similar fraction of red sequence galaxies that evolved through a starburst. Filament SBGs and their outcomes are therefore an important path of galaxy evolution in and around clusters, even if they do not represent the dominant channel to move galaxies from the blue cloud to the red sequence, since the observed fraction of PSBGs in clusters is too small (De Lucia et al. 2009).

The relative numbers of SBGs and PSBGs probably reflects the relative durations of the starburst and post-starburst phases, that is $\sim 1/3$ – $1/2$. If the post-starburst phase typically lasts ~ 1 Gyr (Hogg et al. 2006; Goto 2007), this ratio implies that the starburst phase lasts ~ 0.4 Gyr, close to recent estimates (McQuinn et al. 2010). As a consequence, the SBG infall speed (~ 1 Mpc/Gyr in projection) is insufficient for them to travel along the whole filament into the cluster before the starburst

phase is over, so they enter the cluster as PSBGs (or, maybe, AGNs). We do however observe SBGs in cluster cores. How do they originate? Part of them are likely to be found in the center only because of projection effects. Part of them may form in subclusters as they are tidally compressed by the cluster gravitational field (Oemler et al. 2009). Since the accretion of groups (i.e. subclusters) in clusters increases with z (Ellingson et al. 2001; van den Bosch 2002), higher- z clusters are expected to display a higher fraction of SBGs in their central regions, as indeed found by Dressler et al. (2009).

As far as the evolution of the IR LF is concerned, our results confirm the results of Bai et al. (2009), namely that the number density of IR-emitting galaxies in clusters increases with z at all L_{IR} . Similarly, the total SFR of cluster galaxies per cluster mass also increases with z (Geach et al. 2006; Bai et al. 2009), at least until $z \approx 0.4$ (see Fig. 17). As suggested by Finn et al. (2010), this evolution is likely to result from the combination of a general decline in the SFR of field galaxies (consequence of the gradual exhaustion of their gas reservoirs) coupled to a decrease in the infall rate of field galaxies into clusters (Ellingson et al. 2001; van den Bosch 2002) and to a quenching process at work in the cluster environment, presumably ram-pressure stripping (Gunn & Gott 1972; Quilis et al. 2000).

This evolution appears to accelerate at $z \lesssim 0.4$ as expected if it is linked to the accretion rate of field galaxies, which peaks at relatively low- z for cluster-sized halos (van den Bosch 2002). More data are needed to confirm that the evolution is indeed accelerated at $z \lesssim 0.4$. The current sample of clusters on which the relation of Bai et al. (2009) is based is not complete, and we cannot exclude that the clusters that show excess star formation at $0.2 \lesssim z \lesssim 0.4$ may be a biased set. If all these clusters are currently undergoing mergers, their excess of star formation may be interpreted as the result of contaminating the pristine cluster galaxy population with the presumably younger galaxy population of infalling groups (Chung et al. 2010). A detailed dynamical analysis of the A1763 cluster will be the subject of a forthcoming paper in this series, but indications that this cluster is far from relaxation have already been provided in Paper 0.

In summary, the evolution of the number density of IR-emitting galaxies in cluster cores could result from the competing processes of accretion of star-forming field galaxies, and quenching. It is possible that most IR-emitting galaxies in cluster cores are star-forming galaxies recently infallen from the field that have not yet spent sufficient time in the cluster environment for their star-formation to be quenched. The radially elongated orbits of star forming galaxies in clusters is also suggestive of their recent infall (Biviano & Katgert 2004). If the quenching process is fast enough, one expects to see an environmental dependence of the fraction of IR-emitting galaxies but not of their intrinsic properties. This is what is indicated by the similarities of the sSFR- M_\star relations (see Fig. 14), of the distributions of galaxies in SED classes (see Fig. 15), and of the shape of the IR LFs (see Table 1; see also the results of Haines et al. 2011a, for the Shapley supercluster) across the different supercluster regions.

5. Summary and conclusions

We determine the IR LF of the A1763 supercluster of star-forming galaxies at $z \approx 0.23$. Supercluster members are selected in a sample of 24- μm -detected sources on the basis of their spectroscopic and photometric redshifts. Total L_{IR} and M_\star for supercluster members are obtained by fitting their SEDs. AGNs are identified by their SEDs and other methods (see Paper 2) and

their contribution removed from the IR LFs. Comparison with L_{IR} -estimates obtained from monochromatic $24\ \mu\text{m}$ luminosities shows that a good photometric coverage of the galaxy SEDs is important for accurate L_{IR} -estimates.

We show that the IR LF changes according to the supercluster environment. We define three environments: the cluster core, the large-scale filament, and the cluster outskirts, in order of decreasing galaxy density. By normalizing the IR LFs with the average number densities of optically-selected galaxies, we show that the filament hosts the highest fraction of IR-emitting galaxies at all L_{IR} . Similarly, the filament region contains the highest total SFR per unit galaxy. At the other extreme lies the core region, where LIRGs are almost absent. The IR LF of the cluster outskirts (excluding the filament region) is intermediate between those of the filament and the core.

We do not find any environmental dependence of the $\text{sSFR}-M_{\star}$ relation. Most high-star forming galaxies in the supercluster are also massive, and the excess population of LIRGs in the filament region is due to massive galaxies with normal sSFRs for their M_{\star} , that is to say, relatively low sSFRs.

Galaxies of the different regions have very similar fractions of SED-classes. Normal, SFGs dominate; SBGs dominate at the bright end of the IR LF; AGNs contribute only $\sim 10\%$ in fraction.

Comparison with previous results from the literature confirms the evolution of cluster IR LF found by Bai et al. (2009), as well as the evolution of total cluster SFR divided by cluster mass (Geach et al. 2006; Bai et al. 2009; Chung et al. 2010). The evolution is faster at $z \lesssim 0.4$ than at higher z , unless the clusters that have so far been investigated in the IR at $0.2 \lesssim z \lesssim 0.4$ are a biased set of dynamically young systems, in which the presence of infalling groups biases the estimates of total cluster SFR high.

We discuss these results by drawing a scenario for the evolution of galaxies in and around clusters. Massive star-forming galaxies exist in medium-density environments at $z \sim 0.2$; about two-thirds of them have a mode of star formation resembling that of normal late-type galaxies. As these galaxies enter the cluster environment, they suffer ram-pressure stripping and evolve into passive galaxies. The remaining fraction is undergoing or has recently experienced starbursts, probably induced by galaxy-galaxy interactions (or mergers). They enter the cluster as PSBGs. Together, these two paths of galaxy evolution lead to the build-up of the red sequence in clusters.

In future papers of this series, we will present the spectroscopic catalog of the A1763 region and the new UV data we have obtained from *GALEX* observations; we will investigate the dynamics of the A1763 cluster and the spectral properties of the galaxies in the A1763 supercluster. We also plan to determine morphologies for A1763 supercluster galaxies, and to deepen our investigation into the low- L_{IR} regime with *Herschel* satellite observations.

Acknowledgements. We warmly thank the anonymous referee for the careful reports that have helped us to significantly improve this paper. We acknowledge useful discussions with Sun Mi Chung, Nicholas Lee, Claudia Maraston, Paola Popesso, George Rieke, and Laura Silva. AB and FD acknowledge the hospitality of IPAC at Caltech, and AB also the hospitality of the Institut d'Astrophysique de Paris, during the preparation of this work.

Partial financial support for this research has been provided by the Agenzia Spaziale Italiana through the projects "IR studies of clusters of galaxies from $z = 3$ to $z = 0$ ", and "Star formation in galaxy superclusters with *GALEX*", and by NASA through an award issued by JPL/Caltech.

This research has made use of NASA's Astrophysics Data System, of NED, which is operated by JPL/Caltech, under contract with NASA, and of SDSS, which has been funded by the Sloan Foundation, NSF, the US Department of Energy, NASA, the Japanese Monbukagakusho, the Max Planck Society, and

the Higher Education Funding Council of England. The SDSS is managed by the participating institutions (www.sdss.org/collaboration/credits.html).

References

- Babbedge, T. S. R., Rowan-Robinson, M., Vaccari, M., et al. 2006, *MNRAS*, 370, 1159
- Bai, L., Marcellac, D., Rieke, G. H., et al. 2007, *ApJ*, 664, 181
- Bai, L., Rieke, G. H., Rieke, M. J., Christlein, D., & Zabludoff, A. I. 2009, *ApJ*, 693, 1840
- Bai, L., Rieke, G. H., Rieke, M. J., et al. 2006, *ApJ*, 639, 827
- Barnes, J. E. 1992, *ApJ*, 393, 484
- Barrena, R., Biviano, A., Ramella, M., Falco, E. E., & Seitz, S. 2002, *A&A*, 386, 816
- Beers, T. C., Flynn, K., & Gebhardt, K. 1990, *AJ*, 100, 32
- Bell, E. F., McIntosh, D. H., Katz, N., & Weinberg, M. D. 2003, *ApJS*, 149, 289
- Bernardi, M., Shankar, F., Hyde, J. B., et al. 2010, *MNRAS*, 404, 2087
- Biviano, A. 2008, *arXiv:0811.3535*
- Biviano, A., Durret, F., Gerbal, D., et al. 1996, *A&A*, 311, 95
- Biviano, A. & Katgert, P. 2004, *A&A*, 424, 779
- Biviano, A., Metcalfe, L., McBreen, B., et al. 2004, *A&A*, 425, 33
- Biviano, A., Murante, G., Borgani, S., et al. 2006, *A&A*, 456, 23
- Biviano, A. & Poggianti, B. M. 2009, *A&A*, 501, 419
- Bothwell, M. S., Kennicutt, R. C., Johnson, B. D., et al. 2011, *arXiv:1104.0929*
- Boué, G., Durret, F., Adams, C., et al. 2008, *A&A*, 489, 11
- Braglia, F., Pierini, D., & Böhringer, H. 2007, *A&A*, 470, 425
- Braglia, F. G., Pierini, D., Biviano, A., & Böhringer, H. 2009, *A&A*, 500, 947
- Brammer, G. B., van Dokkum, P. G., & Coppi, P. 2008, *ApJ*, 686, 1503
- Bushouse, H. A. 1987, *ApJ*, 320, 49
- Butcher, H. & Oemler, Jr., A. 1984, *ApJ*, 285, 426
- Calzetti, D., Armus, L., Bohlin, R. C., et al. 2000, *ApJ*, 533, 682
- Cavagnolo, K. W., Donahue, M., Voit, G. M., & Sun, M. 2009, *ApJS*, 182, 12
- Chung, S. M., Gonzalez, A. H., Clowe, D., Markevitch, M., & Zaritsky, D. 2010, *ApJ*, 725, 1536
- Coia, D., McBreen, B., Metcalfe, L., et al. 2005a, *A&A*, 431, 433
- Coia, D., Metcalfe, L., McBreen, B., et al. 2005b, *A&A*, 430, 59
- Collister, A. A. & Lahav, O. 2004, *PASP*, 116, 345
- Cowie, L. L., Barger, A. J., Fomalont, E. B., & Capak, P. 2004, *ApJ*, 603, L69
- da Cunha, E., Eminian, C., Charlot, S., & Blaizot, J. 2010, *MNRAS*, 403, 1894
- Davies, J. I., Baes, M., Bendo, G. J., et al. 2010, *A&A*, 518, L48
- De Lucia, G., Poggianti, B. M., Halliday, C., et al. 2009, *MNRAS*, 400, 68
- DeGroot, M. 1987, *Probability and Statistics*, Second Edition (Addison-Wesley Publishing Co., Reading, MA)
- den Hartog, R. & Katgert, P. 1996, *MNRAS*, 279, 349
- D'Onghia, E., Vogelsberger, M., Faucher-Giguere, C., & Hernquist, L. 2010, *ApJ*, 725, 353
- Dressler, A., Rigby, J., Oemler, A., et al. 2009, *ApJ*, 693, 140
- Duc, P.-A., Fadda, D., Poggianti, B., et al. 2004, in *IAU Colloq. 195: Outskirts of Galaxy Clusters: Intense Life in the Suburbs*, ed. A. Diaferio, 347–351
- Duc, P.-A., Poggianti, B. M., Fadda, D., et al. 2002, *A&A*, 382, 60
- Edwards, L. O. V., Fadda, D., Biviano, A., & Marleau, F. R. 2010a, *AJ*, 139, 434 (Paper 1)
- Edwards, L. O. V., Fadda, D., Frayer, D. T., Lima Neto, G. B., & Durret, F. 2010b, *AJ*, 140, 1891 (Paper 2)
- Efron, B. & Tibshirani, R. 1986, *Stat. Sci.*, 1, 54
- Ellingson, E., Lin, H., Yee, H. K. C., & Carlberg, R. G. 2001, *ApJ*, 547, 609
- Emonts, B. H. C., Morganti, R., Tadhunter, C. N., et al. 2006, *A&A*, 454, 125
- Fadda, D., Biviano, A., Marleau, F. R., Storrie-Lombardi, L. J., & Durret, F. 2008, *ApJ*, 672, L9 (Paper 0)
- Fadda, D., Elbaz, D., Duc, P.-A., et al. 2000, *A&A*, 361, 827
- Fadda, D., Girardi, M., Giuricin, G., Mardirossian, F., & Mezzetti, M. 1996, *ApJ*, 473, 670
- Fadda, D., Marleau, F. R., Storrie-Lombardi, L. J., et al. 2006, *AJ*, 131, 2859
- Fadda, D., Yan, L., Lagache, G., et al. 2010, *ApJ*, 719, 425
- Fasano, G. & Franceschini, A. 1987, *MNRAS*, 225, 155
- Finn, R. A., Desai, V., Rudnick, G., et al. 2010, *ApJ*, 720, 87
- Fisher, D., Fabricant, D., Franx, M., & van Dokkum, P. 1998, *ApJ*, 498, 195
- Fontana, A., Pozzetti, L., Donnarumma, I., et al. 2004, *A&A*, 424, 23
- Gallazzi, A., Bell, E. F., Wolf, C., et al. 2009, *ApJ*, 690, 1883
- Gao, L., Navarro, J. F., Cole, S., et al. 2008, *MNRAS*, 387, 536
- Gavazzi, G. 2009, in *Revista Mexicana de Astronomía y Astrofísica Conference Series*, Vol. 37, 72–78
- Geach, J. E., Smail, I., Ellis, R. S., et al. 2006, *ApJ*, 649, 661
- Geach, J. E., Smail, I., Moran, S. M., Treu, T., & Ellis, R. S. 2009, *ApJ*, 691, 783
- Goto, T. 2007, *MNRAS*, 381, 187
- Goto, T., Arnouts, S., Malkan, M., et al. 2011, *MNRAS*, 414, 1903
- Gunn, J. E. & Gott, J. R. 1972, *ApJ*, 176, 1

- Haines, C. P., Busarello, G., Merluzzi, P., et al. 2011a, *MNRAS*, 412, 127
- Haines, C. P., Busarello, G., Merluzzi, P., et al. 2011b, *MNRAS*, 412, 145
- Haines, C. P., Smith, G. P., Egami, E., et al. 2009a, *ApJ*, 704, 126
- Haines, C. P., Smith, G. P., Egami, E., et al. 2009b, *MNRAS*, 396, 1297
- Haines, C. P., Smith, G. P., Pereira, M. J., et al. 2010, *A&A*, 518, L19
- Harrison, E. R. & Noonan, T. W. 1979, *ApJ*, 232, 18
- Hickox, R. C., Jones, C., Forman, W. R., et al. 2009, *ApJ*, 696, 891
- Hogg, D. W., Masjedi, M., Berlind, A. A., et al. 2006, *ApJ*, 650, 763
- Hwang, H. S., Elbaz, D., Lee, J. C., et al. 2010, *A&A*, 522, A33+
- Katgert, P., Biviano, A., & Mazure, A. 2004, *ApJ*, 600, 657
- Kennicutt, Jr., R. C. 1998, *ARA&A*, 36, 189
- Knobel, C., Lilly, S. J., Iovino, A., et al. 2009, *ApJ*, 697, 1842
- Kodama, T., Balogh, M. L., Smail, I., Bower, R. G., & Nakata, F. 2004, *MNRAS*, 354, 1103
- Koyama, Y., Kodama, T., Shimasaku, K., et al. 2010, *MNRAS*, 403, 1611
- Koyama, Y., Kodama, T., Shimasaku, K., et al. 2008, *MNRAS*, 391, 1758
- Krick, J. E., Surace, J. A., Thompson, D., et al. 2009, *ApJ*, 700, 123
- Kroupa, P. 2001, *MNRAS*, 322, 231
- Lee, N., Le Floc'h, E., Sanders, D. B., et al. 2010, *ApJ*, 717, 175
- Makino, J. & Hut, P. 1997, *ApJ*, 481, 83
- Mamon, G. 1996, in *Third Paris Cosmology Colloquium*, ed. H. J. de Vega & N. Sánchez, 95, arXiv:astro-ph/9511101
- Mamon, G. A., Biviano, A., & Murante, G. 2010, *A&A*, 520, A30
- Maraston, C. 2005, *MNRAS*, 362, 799
- Mauduit, J.-C. & Mamon, G. A. 2007, *A&A*, 475, 169
- McQuinn, K. B. W., Skillman, E. D., Cannon, J. M., et al. 2010, *ApJ*, 721, 297
- Merluzzi, P., Mercurio, A., Haines, C. P., et al. 2010, *MNRAS*, 402, 753
- Metcalfe, L., Fadda, D., & Biviano, A. 2005, *Space Science Reviews*, 119, 425
- Metcalfe, L., Kneib, J.-P., McBreen, B., et al. 2003, *A&A*, 407, 791
- Meusinger, H., Brunzendorf, J., & Krieg, R. 2000, *A&A*, 363, 933
- Moore, B., Katz, N., Lake, G., Dressler, A., & Oemler, Jr., A. 1996, *Nature*, 379, 613
- Murakami, H., Baba, H., Barthel, P., et al. 2007, *PASJ*, 59, 369
- Navarro, J. F., Frenk, C. S., & White, S. D. M. 1997, *ApJ*, 490, 493
- Negroponte, J. & White, S. D. M. 1983, *MNRAS*, 205, 1009
- Oemler, A., Dressler, A., Kelson, D., et al. 2009, *ApJ*, 693, 152
- Oliver, S., Frost, M., Farrah, D., et al. 2010, *MNRAS*, 405, 2279
- Oyaizu, H., Lima, M., Cunha, C. E., et al. 2008, *ApJ*, 674, 768
- Peacock, J. A. 1983, *MNRAS*, 202, 615
- Peng, Y., Lilly, S. J., Kovač, K., et al. 2010, *ApJ*, 721, 193
- Pereira, M. J., Haines, C. P., Smith, G. P., et al. 2010, *A&A*, 518, L40
- Pilbratt, G. L., Riedinger, J. R., Passvogel, T., et al. 2010, *A&A*, 518, L1
- Polletta, M., Tajer, M., Maraschi, L., et al. 2007, *ApJ*, 663, 81
- Porter, S. C. & Raychaudhury, S. 2007, *MNRAS*, 375, 1409
- Porter, S. C., Raychaudhury, S., Pimblet, K. A., & Drinkwater, M. J. 2008, *MNRAS*, 388, 1152
- Quilis, V., Moore, B., & Bower, R. 2000, *Science*, 288, 1617
- Quintana, H., Ramirez, A., & Way, M. J. 1996, *AJ*, 112, 36
- Rawle, T. D., Chung, S. M., Fadda, D., et al. 2010, arXiv:1005.3822
- Rex, M., Rawle, T. D., Egami, E., et al. 2010, *A&A*, 518, L13+
- Rieke, G. H., Alonso-Herrero, A., Weiner, B. J., et al. 2009, *ApJ*, 692, 556
- Rujopakarn, W., Eisenstein, D. J., Rieke, G. H., et al. 2010, *ApJ*, 718, 1171
- Saintonge, A., Tran, K.-V. H., & Holden, B. P. 2008, *ApJ*, 685, L113
- Sanders, D. B., Soifer, B. T., Elias, J. H., et al. 1988, *ApJ*, 325, 74
- Schechter, P. 1976, *ApJ*, 203, 297
- Silva, L., Granato, G. L., Bressan, A., & Danese, L. 1998, *ApJ*, 509, 103
- Spitzer, L. J. & Baade, W. 1951, *ApJ*, 113, 413
- Temporin, S., Duc, P., Ilbert, O., & XMM-LSS/SWIRE collaboration. 2009, *Astronomische Nachrichten*, 330, 915
- Teyssier, R., Chapon, D., & Bournaud, F. 2010, *ApJ*, 720, L149
- Tran, K., Saintonge, A., Moustakas, J., et al. 2009, *ApJ*, 705, 809
- Umemura, M., Fukue, J., & Mineshige, S. 1999, *Advances in Space Research*, 23, 1095
- van den Bosch, F. C. 2002, *MNRAS*, 331, 98
- Werner, M. W., Roellig, T. L., Low, F. J., et al. 2004, *ApJS*, 154, 1
- Wild, V., Walcher, C. J., Johansson, P. H., et al. 2009, *MNRAS*, 395, 144
- Wojtak, R., Łokas, E. L., Mamon, G. A., et al. 2007, *A&A*, 466, 437
- Yahil, A. & Vidal, N. V. 1977, *ApJ*, 214, 347
- Younger, J. D., Hayward, C. C., Narayanan, D., et al. 2009, *MNRAS*, 396, L66
- Zucca, E., Bardelli, S., Bolzonella, M., et al. 2009, *A&A*, 508, 1217